Control of meiotic entry by dual inhibition of a key mitotic transcription factor

Amanda J. Su[1], Siri C. Yendluri[1] and Elçin Ünal[1, §]

[1] Department of Molecular and Cell Biology, University of California, Berkeley, CA, United States, 94720

[§] Lead contact: elcin@berkeley.edu

Keywords: meiosis, mitosis, transcription, cell cycle, LUTI, uORF, Ime1, Swi4, SBF, Whi5, Rb, E2F

Abbreviations: SBF (Swi4/6 cell cycle box [SCB] Binding Factor); MBF (Mlu1 cell cycle box [MCB] Binding Factor); LUTI (Long Undecoded Transcript Isoform); TF (Transcription Factor)

HIGHLIGHTS

- SBF subunit Swi4 is downregulated at meiotic entry by the LUTI-based mechanism
- *SWI4*^{LUTI} and Whi5 work together to inhibit SBF at meiotic entry
- SBF and Ime1 TFs antagonize each other, ensuring mutually exclusive cell states
- SBF-target G1 cyclins block meiosis by preventing Ime1-Ume6 interaction

SUMMARY

The mitosis to meiosis transition requires dynamic changes in gene expression, but whether and how the mitotic transcriptional machinery is regulated during this transition is unknown. In budding yeast, SBF and MBF transcription factors initiate the mitotic gene expression program. Here, we report two mechanisms that work together to restrict SBF activity during meiotic entry: repression of the SBF-specific Swi4 subunit through LUTI-based regulation and inhibition of SBF by Whi5, a functional homolog of the Rb tumor suppressor. We find that untimely SBF activation causes downregulation of early meiotic genes and delays meiotic entry. These defects are largely driven by the SBF-target G1 cyclins, which block the interaction between the central meiotic regulator Ime1 and its cofactor Ume6. Our study provides insight into the role of *SWI4*^{LUTI} in establishing the meiotic transcriptional program and demonstrates how the LUTI-based regulation is integrated into a larger regulatory network to ensure timely SBF activity.

INTRODUCTION

A key aspect in understanding developmental programs and cell state transitions is mapping the interplay between transcription factors and their associated gene regulatory networks. In the budding yeast *Saccharomyces cerevisiae*, the transition from mitotic growth to meiotic differentiation is a crucial decision that is regulated by multiple inputs, such as nutrient availability, respiration competence, and cell identity. Under nutrient-limiting conditions, a diploid cell enters the meiotic program to produce four haploid gametes. The process of meiotic entry is tightly controlled by the master transcriptional regulator Ime1, as both extrinsic (e.g. nutrient status, extracellular pH) and intrinsic (e.g. mating type, mitochondrial function) cues are integrated at the *IME1* promoter (Kassir et

al., 1988; Honigberg, 2003; reviewed in van Werven and Amon, 2011). Once translated, Ime1 is phosphorylated by the Rim11 and Rim15 kinases to promote its nuclear localization and interaction with Ume6 (Vidan and Mitchell, 1997; Pnueli et al., 2004; Malathi et al., 1999, 1997). In mitotically dividing cells, Ime1 target genes are repressed by Ume6 through its association with the Sin3-Rpd3 histone deacetylase complex (Kardosh and Struhl, 1997; Rundlett E. et al., 2003). However, under nutrient starvation, entry into the meiotic program is initiated by the interaction between Ime1 and Ume6, which together function as a transcriptional activator, culminating in the induction of early meiotic genes (Bowdish et al., 1995; Harris and Ünal, 2023). Mitosis to meiosis transition requires dynamic remodeling of the gene regulatory networks to maintain the mutual exclusivity of these programs. While entry into the mitotic program is initiated by the central transcription factors SBF and MBF (Spellman et al., 1998; Iyer et al., 2001), whether and how these complexes are regulated during meiotic entry is unknown.

The molecular mechanisms regulating entry into the mitotic cell cycle, also known as G1/S transition, are functionally conserved from yeast to metazoans (reviewed in Van Den Heuvel and Dyson, 2008). SBF and MBF are heterodimeric transcription factors composed of Swi4-Swi6 and Mbp1-Swi6 subunits, respectively (Figure 1A). Though there is no sequence homology these transcription factors are functionally homologous to the mammalian E2Fs. E2Fs are negatively regulated by the tumor suppressor protein Rb, which is homologous to the budding yeast Whi5 that inhibits SBF in early G1 (De Bruin et al., 2004; Costanzo et al., 2004; Hasan et al., 2014). Whi5-based SBF inhibition is relieved by cyclin/CDK-dependent phosphorylation and subsequent re-localization of

74 Whi5 from the nucleus to the cytoplasm (Wagner et al., 2009). Although SBF and MBF
75 act in parallel during the G1/S transition (Spellman et al., 1998; Iyer et al., 2001), they
76 activate functionally specialized subsets of gene targets. SBF regulates the expression
77 of genes involved in budding and cell morphogenesis, while MBF-regulated genes are
78 involved in DNA replication and repair (Iyer et al., 2001; Simon et al., 2001). Despite the
79 well-characterized function in budding yeast mitotic growth, the regulation and function of
80 SBF and MBF during meiotic entry remains largely unknown. In contrast to mitotic
81 divisions where budding and DNA replication occur simultaneously, the meiotic program
82 requires DNA replication and repair, but not bud morphogenesis or asymmetric growth.
83 Accordingly, the regulation and subsequent activity of SBF and MBF are likely to be
84 divergent to establish meiotic entry.
85
86 The activity of SBF and MBF is regulated in part through subunit abundance, which in
87 turn controls expression of the G1/S regulon (Dorsey et al., 2018). For example,
88 overexpression of a hyperactive allele of *SWI4* can trigger premature entry into the cell
89 cycle (Sidorova and Breeden, 2002). Additionally, *SWI4* has also been shown to be
90 haploinsufficient and rate limiting during G1/S progression (Mcinerny et al., 1997). These
91 results suggest that the precise levels of SBF and MBF subunits are important for
92 activating the G1/S regulon at the correct time.
93
94 Three key observations support differential regulation of SBF and MBF during the meiotic
95 program: First, a meiotic mass spectrometry dataset suggests that Swi4 has dynamic
96 protein behavior, which is not observed for its counterparts Swi6 and Mbp1 (Cheng et al.,

97 2018). Second, meiotic cells express a non-canonical mRNA from the *SWI4* locus called
98 LUTI (Brar et al., 2012; Tresenrider et al., 2021), which stands for Long Undecoded
99 Transcript Isoform (Chen et al., 2017; Chia et al., 2017). Third, two SBF-specific targets,
100 namely the G1-cyclins *CLN1* and *CLN2*, have been shown to repress early meiotic gene
101 expression (Colomina et al., 1999).
102
103 LUTI-based gene regulation repurposes gene-activating transcription factors as
104 repressors by a two-pronged mechanism (Chen et al., 2017; Chia et al., 2017; Tresenrider
105 and Ünal, 2017; Tresenrider et al., 2021). First, transcription factor-dependent activation
106 of the LUTI promoter results in co-transcriptional silencing of the downstream canonical
107 gene promoter. Second, the coding sequence (CDS) within the LUTI is translationally
108 repressed due to competitive translation of the upstream open reading frames (uORFs)
109 in the LUTI-specific 5′ leader. Consequently, upregulation of the LUTI results in
110 downregulation of the canonical mRNA and corresponding protein. While LUTIs are
111 conserved from yeast to humans and have been identified in different cellular contexts
112 (Cheng et al., 2018; Van Dalfsen et al., 2018; Hollerer et al., 2019; Jorgensen et al., 2020),
113 their biological significance remains poorly understood. In fact, only a single LUTI has
114 been assigned a biological role so far with distinct phenotypic outcomes resulting from its
115 loss or gain of function (Chen et al., 2017; Chia et al., 2017).
116
117 In this study, we aimed to investigate the differential regulation of SBF and MBF during
118 the meiotic program and determine how the untimely activation of SBF impacts meiotic
119 entry. We found that overexpression of Swi4 results in the activation of SBF targets and

120 concomitant downregulation of the early meiotic genes. SBF targets Cln1 and Cln2 inhibit
121 meiotic entry by blocking the interaction between Ime1 and its cofactor Ume6.
122 Furthermore, the LUTI-based mechanism causes downregulation of Swi4 protein
123 synthesis and acts in conjunction with Whi5 to restrict SBF activity during meiosis.
124 Overall, our study reveals the functional role of a LUTI in establishing the early meiotic
125 transcriptome, demonstrates how the LUTI-based regulation is integrated into a larger
126 regulatory network to ensure timely SBF activity, and provides mechanistic insights into
127 how SBF misregulation impedes transition from mitotic to meiotic cell fate.
128

129 **RESULTS**

130 **Swi4 is the sole downregulated subunit within the SBF and MBF complexes during**
131 **meiosis**

132 While the SBF and MBF transcription factors have been heavily studied in the context of
133 the mitotic cell cycle, their involvement in regulating the meiotic transcriptional program is
134 not well understood. To understand the regulation and function of these complexes during
135 meiosis, we first monitored the levels of SBF and MBF subunits throughout a meiotic time
136 course. Cells were first grown in rich media overnight and were then transferred to pre-
137 sporulation media. After additional overnight growth, cells were shifted to sporulation
138 media (SPO) to induce meiosis, and samples were taken hourly for protein extraction and
139 immunoblotting to monitor the abundance of each subunit. Unlike the mitotic G1/S
140 transition (Kelliher et al., 2018), meiotic entry resulted in ~30% decrease in Swi4 levels
141 after 2 hours, while Mbp1 and Swi6 levels were increased (Figure 1B and 1C*)*. These
142 data indicate that Swi4 is the sole subunit within SBF and MBF whose level declines

143 during meiotic entry and are consistent with a published mass spectrometry dataset
144 (Cheng et al., 2018).
145
146 We next examined the expression of a set of well-characterized transcripts that are
147 regulated by SBF or MBF (Iyer et al., 2001; Simon et al., 2001; Bean et al., 2005; Harris
148 et al., 2013; Smolka et al., 2012) using a published meiotic RNA-seq dataset (Brar et al.,
149 2012). This analysis revealed that compared to mitotically dividing cells, most of the SBF-
150 specific target genes had either low or no expression during early meiosis (Figure 1D). In
151 contrast, most of the MBF targets displayed increased expression upon meiotic entry
152 (Figure 1D).
153
154 Based on our findings thus far, we propose that Swi4 levels are downregulated in meiosis
155 to ensure that SBF targets, including *CLN1* and *CLN2*, are turned off during meiotic entry.
156 If so, then higher Swi4 levels should lead to increased expression of SBF targets. To test
157 this possibility, we overexpressed *SWI4* by placing it under the regulation of the *ATG8*
158 promoter (*pATG8-SWI4*), which is highly expressed in meiosis (Brar et al., 2012). The
159 steady-state level of *pATG8*-driven Swi4 was 5 times higher than wild type (Figure S1A
160 and S1B). Using reverse transcription coupled with quantitative polymerase chain
161 reaction (RT-qPCR), we measured the transcript levels of well-characterized SBF targets
162 and observed a significant increase in the expression of *CLN1* and *CLN2* in *pATG8-SWI4*
163 cells relative to wild type (Figure 1E, $p = 0.0351$ [*CLN1*], $p = 0.0013$ [*CLN2*], two-tailed t-
164 test). In contrast, the MBF-specific targets *CDC21* and *RNR1* remained similar (Figure
165 1E, $p = 0.8488$ [*CDC21*], $p = 0.0859$ [*RNR1*], two-tailed t-test). These findings indicate

166 that upregulation of *SWI4* is sufficient to induce the expression of SBF-specific targets
167 *CLN1* and *CLN2* in meiosis without affecting MBF-specific targets.
168
169 To test whether the downregulation of *SWI4* is functionally important for meiotic
170 progression, we used time-lapse fluorescence microscopy and visualized the kinetics of
171 meiotic divisions in *pATG8-SWI4* cells relative to wild type. By tracking the endogenous
172 histone H2B fused to the red fluorescent protein mCherry (Htb1-mCherry), we found that
173 *SWI4* overexpression caused a significant delay in meiotic progression (Figure 1F, $p =$
174 0.0045, Mann-Whitney test). We conclude that downregulation of *SWI4* is necessary for
175 timely meiotic progression.
176
177 **Regulation of Swi4 abundance is required for timely meiotic entry**
178 Since Swi4 abundance, and by inference SBF activity, was decreased during the mitosis-
179 to-meiosis transition, we hypothesized that the meiotic progression delay observed in
180 *pATG8-SWI4* cells was due to meiotic entry defects. To test this we monitored Ime1, a
181 meiosis-specific transcription factor and a master regulator of meiotic entry (Kassir et al.,
182 1988; Honigberg, 2003; reviewed in van Werven and Amon, 2011). To quantify the bulk
183 levels of Ime1 protein in meiosis, we performed immunoblotting. During meiotic entry (2
184 h in SPO), when Swi4 abundance was elevated, there was a 50% reduction in Ime1 levels
185 in *pATG8-SWI4* cells compared to wild type (Figure S1C and S1D). In parallel, we
186 monitored meiotic entry on a single-cell basis by measuring the localization of
187 endogenous Ime1 carrying an N-terminal green fluorescent protein tag (*GFP-IME1*;
188 Moretto 2018) and Htb1-mCherry. Compared to wild type where > 90% of the cells had

189 nuclear Ime1 following meiotic entry (2 h in SPO), only ~50% of *pATG8-SWI4* cells had
190 nuclear Ime1, which was significantly lower (Figure 2A and 2B, $p = 0.0169$, two-tailed t-
191 test).
192
193 Given that the increase in Swi4 levels coincided with a decrease in Ime1 protein
194 expression and nuclear localization, this raised the possibility that Swi4 interferes with
195 Ime1 function. To further investigate the relationship between these two transcription
196 factors at a single-cell level, we generated strains carrying endogenous fluorescent
197 protein tags for each transcription factor (*GFP-IME1, SWI4-mCherry*). Using DAPI as a
198 nuclear marker, we measured the mean nuclear intensity of each transcription factor
199 before (0 h) and after meiotic entry (4 h) (see Materials and Methods for details on image
200 quantification). In wild type, most cells exhibited decreased nuclear Swi4 and increased
201 nuclear Ime1 upon meiotic entry (Figure 2C-E). Conversely, in the *pATG8-SWI4* mutant,
202 there was a significant shift in the fraction of cells with higher nuclear Swi4 levels (Figure
203 2D and 2E, $p < 0.0001$, Mann-Whitney test,). Additionally, the cells with increased nuclear
204 Swi4 had reduced levels of nuclear Ime1 (Figure 2E, $p < 0.0001$, Mann-Whitney test).
205 This inverse relationship between Swi4 and Ime1 nuclear localization further indicates
206 that higher levels of Swi4 are antagonistic to Ime1 function.
207
208 Ime1 is necessary for the expression of early meiotic genes. Therefore, we next
209 characterized the changes in the early meiotic transcriptome upon *SWI4* overexpression
210 by mRNA-sequencing (mRNA-seq). Using DESeq2 (Love et al., 2014), we identified
211 differentially expressed genes in *pATG8-SWI4* mutant compared to wild type during

212 meiotic entry (2 h in SPO). To investigate general pathways being affected by increased
213 Swi4 levels in meiosis, we ran gene ontology analysis of statistically significant (padj <
214 0.05) output from DESeq2, which revealed that the genes with significantly increased
215 expression were involved in mitosis while those with significantly decreased expression
216 were involved in meiotic processes (Figure S2A and S2B). Regarding the SBF targets,
217 we noticed increased expression of many genes, including *CLN1* and *CLN2* (Figure 2F,
218 Supplemental Table 1). We focused on a cluster of previously identified early meiotic
219 genes involved in DNA replication and recombination (Brar et al., 2012) and observed
220 that more than 50% had a significant decrease in their expression upon *SWI4*
221 overexpression (padj < 0.05, Figure 2F, Supplemental Table 1). Finally, gene set
222 enrichment analysis was performed to test whether expression of either the early meiotic
223 gene set or SBF target gene set is enriched in wild type or *pATG8-SWI4* mutant cells
224 (Subramanian et al., 2005). This gene set level analysis revealed significant enrichment
225 of SBF target gene expression (NES = 2.88, p < 0.001, Figure 2G), as well as significant
226 disenrichment of early meiotic gene expression (NES = -2.88, p < 0.001, Figure 2G) in
227 the *pATG8-SWI4* mutant. Altogether, these findings demonstrate that the increased levels
228 of Swi4 during transition from mitotic to meiotic cell fate abruptly activates SBF and
229 disrupts the early meiotic transcriptome, highlighting the importance of *SWI4* regulation.
230
231 As an orthogonal approach, we performed live-cell imaging of Rec8, endogenously
232 tagged with GFP (Rec8-GFP), which is a meiosis-specific cohesin subunit and a direct
233 transcriptional target of Ime1 (Primig et al., 2000; Klein et al., 1999). Htb1-mCherry was
234 used as a nuclear marker. This analysis revealed a significant delay in Rec8-GFP nuclear

235 appearance in the *pATG8-SWI4* strain compared to wild type (Figure 2H and 2I, p =
236 0.0005, Mann-Whitney test). Furthermore, sporulation efficiency was decreased by ~20%
237 in the *pATG8-SWI4* strain relative to wild type (Supplemental Table 2). These findings
238 are consistent with the mRNA-seq data and further underscore the importance of *SWI4*
239 downregulation in establishing a robust meiotic cell fate.
240

241 **Removal of the SBF targets Cln1 or Cln2 partially rescues the meiotic entry delay**
242 **in *pATG8-SWI4* mutants**

243 Overexpression of the G1 cyclins *CLN1*, *CLN2* and *CLN3* has been previously shown to
244 inhibit meiotic entry (Colomina et al., 1999). Given that *CLN1* and *CLN2* are
245 transcriptional targets of SBF, we next determined whether the meiotic progression delay
246 in *pATG8-SWI4* cells could be due to increased G1 cyclin protein levels. We first
247 examined Cln1 and Cln2 protein levels using epitope-tagged alleles at their endogenous
248 loci (*CLN1-3V5* or *CLN2-3V5*) in wild-type and *pATG8-SWI4* cells. In response to *SWI4*
249 overexpression, we observed up to 2-fold and 10-fold increase in Cln1 and Cln2 protein
250 levels, respectively, corroborating the mRNA-seq data (Figure 3A-D).
251

252 To determine whether these two G1 cyclins are functionally responsible for the meiotic
253 progression delay observed in response to SBF misregulation, we performed time-lapse
254 fluorescence microscopy in cells carrying Rec8-GFP and Htb1-mCherry. We found that
255 deletion of either *CLN1* or *CLN2* significantly rescued the meiotic progression delay in the
256 *pATG8-SWI4* mutant (p = 0.0111 [*cln1*Δ], p = 0.0478 [*cln2*Δ], Mann-Whitney test) (Figure
257 3E and 3F). The kinetics of meiotic entry in the absence of either Cln1 or Cln2 closely

258 resembled that of wild type (Figure S3A), indicating that the observed rescue was specific
259 to the meiotic defect resulting from elevated Swi4 levels. However, *pATG8-SWI4* cells
260 lacking either *CLN1* or *CLN2* were still delayed compared to wild type, suggesting
261 redundancy. We were unable to examine meiotic progression in the *cln1Δ cln2Δ* double
262 mutant due to its severe sickness in the SK1 background. Nevertheless, our analyses
263 establish a causal link demonstrating that both *CLN1* and *CLN2* contribute to the meiotic
264 defects arising from SBF misregulation.
265
266 **Tethering of Ime1 to Ume6 is sufficient to overcome the meiotic block exerted by**
267 **G1 cyclin overexpression**
268 Given the partial rescue of the meiotic delay in *pATG8-SWI4* mutants by the deletion of
269 individual G1 cyclins, we next investigated how the G1 cyclins interfere with meiosis. To
270 this end, we generated transgenes that expressed either *CLN1* or *CLN2* under the control
271 of the *pATG8* promoter for meiotic overexpression. While wild-type cells successfully
272 completed meiosis with more than 94% sporulation efficiency, *CLN2* overexpression
273 resulted in only 8.5% of cells forming gametes. Overexpression of *CLN1* also resulted in
274 a meiotic defect, albeit to a lesser extent than the *pATG8-CLN2* mutant (65% sporulation
275 efficiency, Figure 4A).
276
277 Since the meiotic defect was more pronounced in response to *CLN2* overexpression, we
278 decided to use the *pATG8-CLN2* mutant to explore how G1 cyclins counteract meiosis.
279 To assess meiotic entry, we performed fixed-cell imaging for GFP-Ime1 and found that
280 when *CLN2* was overexpressed, only 5% of the *pATG8-CLN2* cells displayed nuclear

281 GFP-Ime1 signal during early meiosis as opposed to >84% of wild-type cells (Figure 4B
282 and 4C, 2 h in SPO). In parallel, we measured *IME1* transcript and Ime1 protein levels.
283 In both cases, we observed ~30% decrease in abundance in the *pATG8-CLN2* mutant
284 relative to wild type (Figure S4A-C, 2 h in SPO). These data raise the possibility that the
285 meiotic entry defect observed in the *pATG8-CLN2* mutant arises from downregulation of
286 *IME1* expression.
287
288 To test whether the increased levels of Ime1 can rescue the meiotic defect of *pATG8-*
289 *CLN2* mutant, we replaced the endogenous *IME1* promoter with a copper-inducible *CUP1*
290 promoter (Figure 4D). We adapted a previously well-characterized overexpression allele
291 of *IME1*, *pCUP1-IME1,* (Berchowitz et al., 2013; Chia and van Werven, 2016) and
292 included a functional, N-terminal GFP tag to track Ime1's subcellular localization *(pCUP1-*
293 *GFP-IME1*). Use of the *CUP1* promoter was successful in elevating *IME1* transcript and
294 protein levels in the presence of *CLN2* overexpression (Figure S4D-F). Despite the
295 rescue of *IME1* expression, gamete formation was still severely perturbed (Figure 4A).
296 Using a single z-slice to measure mean nuclear intensity, we noticed that the intensity of
297 the nuclear Ime1 signal was significantly lower in the *pATG8-CLN2; pCUP1-GFP-IME1*
298 cells compared to the *pCUP1-GFP-IME1* control (Figure 4E and 4F, $p < 0.0001$, Mann-
299 Whitney test). This finding indicates that rescue of *IME1* expression did not also rescue
300 sporulation, further suggesting a defect in Ime1 nuclear localization. To test this
301 possibility, we utilized a nanobody trap strategy (Fridy et al., 2014) where we C-terminally
302 fused a single-domain anti-GFP antibody to Pus1, a constitutively nuclear localized
303 protein (*PUS1-αGFP*, Figure 4G). In this background, control strains carrying a *GFP-IME1*

304 allele sporulated efficiently, demonstrating that tethering of Ime1 to Pus1 does not
305 interfere with Ime1 function (Figure 4A). Furthermore, mean nuclear intensity of GFP-
306 Ime1 was indistinguishable between *PUS1-αGFP* and *pATG8-CLN2; PUS1-αGFP*,
307 indicating that nuclear localization was fully rescued (Figure 4H and 4I, p = 0.6563 [*PUS1-*
308 *αGFP* vs. *pATG8-CLN2; PUS1-αGFP*], Mann-Whitney test). Surprisingly, these cells still
309 failed to undergo meiosis (Figure 4A), suggesting that G1 cyclins interfere with Ime1
310 function at an additional step beyond misregulating its expression and localization.
311 Alternatively, G1 cyclins could disrupt a different meiotic factor in addition to Ime1.
312
313 To induce early meiotic genes, Ime1 must interact with another transcription factor called
314 Ume6 (Rubin-Bejerano et al., 1996). Since Ime1 itself does not possess a DNA-binding
315 domain, its binding to Ume6 is essential for targeting Ime1 to early meiotic gene
316 promoters (Smith et al., 1993; Rubin-Bejerano et al., 1996). To address whether the G1
317 cyclins might disrupt the interaction between Ime1 and Ume6, we fused the anti-GFP
318 nanobody to Ume6 (*UME6-αGFP*) in the *pATG8-CLN2* strain carrying a GFP tagged Ime1
319 (Figure 4J). This nanobody trap should lead to constitutive tethering of Ime1 to Ume6, as
320 evidenced by the rescue of Ime1 nuclear localization (Figure 4K and 4L, p = 0.035 [wild
321 type vs. *pATG8-CLN2 UME6-αGFP*] Mann-Whitney test). Under these conditions, the
322 sporulation defect of *pATG8-CLN2* mutant was rescued, reaching similar levels to wild
323 type (Figure 4A). Since *IME1* is expressed from its endogenous promoter in the *pATG8-*
324 *CLN2; UME6-αGFP* strain, these data suggest that overexpression of G1 cyclins results
325 in meiotic failure due to reduced Ime1-Ume6 interaction.
326

327 Our findings thus far highlight the biological significance of restricting SBF activity during
328 the transition from mitotic to meiotic cell fate. Among the SBF targets, G1 cyclins pose a
329 major block to meiotic entry by interfering with Ime1 function, critically at the level of Ime1-
330 Ume6 interaction. While our findings emphasize the importance of *SWI4* regulation to
331 ensure timely SBF activity, the question remains as to how SBF activity is downregulated
332 during transition from mitosis to meiosis.
333

334 **Ime1-dependent expression of a LUTI from the *SWI4* locus leads to a reduction in**
335 **Swi4 protein levels during meiotic entry**

336 Given the importance of *SWI4* downregulation in restricting SBF activity during mitotic to
337 meiotic cell fate transition, we next investigated the mechanism of *SWI4* downregulation.
338 A previous study identified a long undecoded transcript isoform (LUTI) expressed from
339 the *SWI4* locus in meiotic cells (Brar et al., 2012, Figure 5A). When $SWI4^{LUTI}$ is expressed,
340 the canonical protein-coding *SWI4* transcript, $SWI4^{canon}$, is downregulated (Tresenrider et
341 al., 2021, Figure 5B), suggesting that LUTI expression restricts Swi4 protein levels and
342 thus SBF activity during meiotic entry.
343

344 To further investigate LUTI-based repression of *SWI4*, we examined the relationship
345 between $SWI4^{LUTI}$ and $SWI4^{canon}$ transcripts using single molecule RNA fluorescence in
346 situ hybridization (smFISH: Chen et al., 2017, 2018; Raj et al., 2008). Two distinct probes
347 were used: one, conjugated to Quasar 670 (Q670) and complementary to the *SWI4*
348 coding sequence (CDS) and the other, conjugated to CAL Fluor Red 590 (CF590) and
349 unique to the 5′ extended LUTI sequence. Accordingly, a spot where the two probe sets

350 colocalized indicated a *SWI4*^{LUTI} transcript, whereas a spot marked with Q670 probe
351 alone highlighted a *SWI4*^{canon} transcript. We used a well-established meiotic cell
352 synchronization system (Berchowitz et al., 2013) to investigate the precise temporal
353 expression of these two mRNA isoforms. In comparison to premeiotic state, meiotic cells
354 displayed a significant increase in *SWI4*^{LUTI} transcripts ($p < 0.0001$, Mann-Whitney test)
355 as well as a significant decrease in *SWI4*^{canon} transcripts ($p = 0.0007$, Mann-Whitney test)
356 (Figure 5C and 5D), thus confirming their inverse expression pattern.
357
358 To characterize the functional contribution of the LUTI to *SWI4* downregulation, we
359 eliminated *SWI4*^{LUTI} production (Δ*LUTI*) by deleting its promoter (Tresenrider et al., 2021)
360 and used RNA blotting to visualize the *SWI4* mRNA isoforms. In wild-type cells, *SWI4*^{LUTI}
361 was readily detectable after 1 hour in SPO, corresponding to early meiotic entry (Figure
362 5E). During the time points when *SWI4*^{LUTI} was highly expressed, *SWI4*^{canon} transcript
363 levels were lower, consistent with the smFISH data. In Δ*LUTI* cells, we observed an
364 increase in the abundance of *SWI4*^{canon} mRNA (Figure 5E). This finding corroborates
365 previous reports, where LUTI expression leads to co-transcriptional silencing of the
366 canonical gene promoter, thereby silencing expression of the protein-coding transcript
367 (Chen et al., 2017; Chia et al., 2017; Van Dalfsen et al., 2018; Tresenrider et al., 2021;
368 Vander Wende et al., 2022). Finally, by immunoblotting, we observed an increase in Swi4
369 protein abundance in the Δ*LUTI* mutant compared to wild type (Figure 5E and 5F), further
370 indicating that *SWI4*^{LUTI} expression downregulates Swi4 protein levels in meiosis.
371

372 *SWI4*^{LUTI} translation occurs within the upstream ORFs (uORFs) of its 5′ leader sequence
373 (Brar et al., 2012). If the uORFs repress productive translation of the *SWI4* CDS contained
374 within the LUTI, then their removal should result in increased Swi4 protein levels. To
375 determine whether the uORFs inhibit translation of the *SWI4* CDS, we mutated the start
376 codon of all seven uORFs within *SWI4*^{LUTI} from ATG to ATC (Δ*uORF*) and measured Swi4
377 protein levels using immunoblotting. Compared to wild type, the Δ*uORF* mutant had
378 higher levels of Swi4 protein (Figure 5G and 5H). RNA blotting confirmed that *SWI4*^{canon}
379 transcript levels remained similar between wild type and Δ*uORF* mutant, whereas
380 *SWI4*^{LUTI} levels were higher in the Δ*uORF* mutant compared to wild type (Figure 5G),
381 likely resulting from increased transcript stability due to bypass of nonsense mediated
382 decay (Tresenrider et al., 2021). Our findings indicate that the uORFs within the LUTI are
383 translated at the expense of *SWI4* CDS, thus halting Swi4 synthesis during early meiosis.
384
385 Our previous findings highlight an antagonistic relationship between Swi4 and Ime1
386 nuclear localization, whereby overexpression of *SWI4* leads to a decrease in Ime1
387 nuclear localization (Figure 2E). Given the previous finding that Ime1 activates
388 transcription of LUTIs in early meiosis (Tresenrider et al., 2021), we were curious whether
389 the reverse regulation could also occur, where Ime1 causes downregulation of Swi4
390 through activating *SWI4*^{LUTI} transcription. To test this possibility, we used an inducible
391 allele of *IME1* (*pCUP1-IME1*) (Chia and van Werven, 2016) and measured Swi4 protein
392 abundance. In the absence of *IME1* induction, Swi4 levels remained constant. However,
393 after 1 hour of *IME1* induction, Swi4 levels started to decrease dramatically (Figure 5I and
394 5J). Therefore, reduction in Swi4 levels is dependent on Ime1 rather than being driven by

395 nutrient deprivation in SPO, a condition that is known to trigger autophagy (Abeliovich
396 and Klionsky, 2001). To further assess whether *SWI4*^{LUTI} is regulated by the Ime1-Ume6
397 transcription factor complex, we analyzed a published Ume6 ChIP-seq dataset
398 (Tresenrider et al., 2021) and found evidence for Ume6 binding at the *SWI4*^{LUTI} promoter
399 (Figure 5K). Additionally, analysis of an mRNA-seq dataset from *UME6-T99N*
400 (Tresenrider et al., 2021), an allele of *UME6* that can no longer interact with Ime1 revealed
401 a dramatic reduction in *SWI4*^{LUTI} expression in meiotic conditions (Figure S5). Together,
402 these data support the notion that Ime1-Ume6 complex induces the expression of
403 *SWI4*^{LUTI}, which in turn inhibits Swi4 protein synthesis through the combined act of
404 transcriptional and translational interference.
405

406 **_SWI4_^{LUTI} is integrated into a larger regulatory network to regulate SBF activity**
407 **during meiotic entry**

408 Since the removal of *SWI4*^{LUTI} resulted in an increase in Swi4 levels, we next wanted to
409 investigate how the loss of LUTI-based regulation affects meiotic entry. We performed
410 mRNA-seq in Δ*LUTI* mutant or wild-type cells during meiotic entry (2 h in SPO) and used
411 DESeq2 to identify differentially expressed genes. To our surprise, there was no obvious
412 increase in the expression of many SBF targets (Figure 6A). Namely, *CLN1* and *CLN2*
413 were both expressed at similar levels to wild type upon loss of *SWI4*^{LUTI}. Therefore, it
414 appears that disruption of the LUTI-based regulation alone is not sufficient to reactivate
415 SBF targets.
416

417 Since transition from the mitotic to meiotic program is a critical cell fate decision, it is likely
418 that additional players are in place to restrict SBF activity. In this case, even when the
419 LUTI-based regulation fails, SBF would remain largely inactive due to a backup
420 mechanism. In support of this notion and consistent with a previous report (Argüello-
421 Miranda et al., 2018), the SBF inhibitor Whi5 was expressed during early meiosis (0 h in
422 SPO) and localized to the nucleus (Figure S6A). During the mitotic G1 phase, Whi5
423 associates with promoter-bound SBF, thereby preventing the transcription of SBF target
424 genes (De Bruin et al., 2004; Costanzo et al., 2004). Shortly before the G1/S transition,
425 phosphorylation of Whi5 via the Cln3/CDK pathway activates SBF by promoting nuclear
426 export of Whi5 (De Bruin et al., 2004; Costanzo et al., 2004). However, in nutrient-
427 deprived conditions that favor meiosis such as nitrogen limitation, *CLN3* is translationally
428 repressed and any Cln3 protein that is expressed is also unstable (Parviz and Heideman,
429 1998; Gallego et al., 1997). Without Cln3/CDK, Whi5 is expected to inhibit SBF in a
430 constitutive manner.
431
432 To determine whether Whi5 and *SWI4*^{LUTI} act in parallel to restrict SBF activity, we
433 removed Whi5 from the nucleus using the anchor-away method, which enables
434 compartment-specific depletion of a target protein via inducible dimerization (Haruki et
435 al., 2008). Whi5 was tagged with FRB and ribosomal protein Rpl13a was tagged with
436 FKBP12. Upon addition of rapamycin, Rpl13a-FKBP12 and Whi5-FRB formed a
437 heterodimer, leading to successful nuclear exclusion of Whi5 (Figure 6B). Using Whi5
438 anchor away (*WHI5-AA)* alone or in combination with removal of LUTI-based *SWI4*
439 regulation (Δ*LUTI)*, we performed mRNA-seq to measure expression of SBF targets and

440 early meiotic genes. Similar to the Δ*LUTI* single mutant, *WHI5-AA* alone did not
441 significantly change the expression of SBF targets or early meiotic genes relative to wild
442 type (Figure 6C). However, loss of both modes of regulation resulted in increased
443 expression of SBF targets as well as a concomitant decrease in early meiotic transcripts
444 compared to wild type (Figure 6D, Supplemental Table 3). As expected, Swi4 levels were
445 similar to wild type in *WHI5-AA* but were elevated in Δ*LUTI* and Δ*LUTI*; *WHI5-AA* mutants
446 (Figure S6B). Gene set enrichment analysis revealed a significant enrichment of the SBF
447 regulon (NES = 1.95, $p < 0.001$) as well as significant disenrichment of the early meiotic
448 genes (NES = -3.39, $p < 0.001$) in the Δ*LUTI*; *WHI5-AA* double mutant (Figure S6C).
449
450 Finally, we monitored meiotic entry using time-lapse fluorescence microscopy in strains
451 carrying endogenously tagged Rec8-GFP in conjunction with Htb1-mCherry. In
452 agreement with our mRNA-seq data, loss of either LUTI- or Whi5-based repression of
453 SBF alone was not sufficient to cause a delay in meiotic entry (Figure 6E). However,
454 simultaneous perturbation of both pathways led to a significant delay in meiotic entry
455 (Figure 6E, $p = 0.0112$, Mann-Whitney test). These data further support the notion that
456 $SWI4^{LUTI}$ is integrated into a larger regulatory network to regulate SBF activity during
457 meiotic entry, which includes Whi5-mediated repression of SBF.
458
459 **DISCUSSION**
460 In this study we describe two distinct mechanisms by which meiotic cells inhibit the activity
461 of SBF, a transcription factor complex crucial for the G1/S transition during the mitotic cell
462 cycle. The dual inhibition of SBF converges on its unique subunit Swi4 and is important

463 for proper transition from mitotic to meiotic cell fate. Swi4 inhibition occurs through: (1)
464 meiosis-specific expression of a LUTI from the *SWI4* locus, *SWI4*^{LUTI}, which
465 downregulates Swi4 protein levels, and (2) repression of Swi4 activity by Whi5, which
466 occurs even when the LUTI-based regulation is disrupted. Conditions that lead to
467 elevation of Swi4 levels at meiotic entry result in abrupt activation of the SBF and a
468 concomitant decline in the expression of early meiotic genes, leading to meiotic
469 progression delays. Additionally, we show that the SBF targets *CLN1* and *CLN2* are major
470 drivers of the meiotic entry defect resulting from SBF misregulation. The *CLN*-dependent
471 phenotypes can be largely rescued by tethering of the central meiotic regulator Ime1 to
472 its cofactor Ume6, suggesting that the primary reason for meiotic failure caused by these
473 G1 cyclins is due to a defect in Ime1-Ume6 interaction. Our findings reveal the functional
474 role of a LUTI in establishing the meiotic transcriptional program, demonstrate how the
475 LUTI-based regulation is integrated into a larger regulatory network to ensure timely SBF
476 activity, and provide mechanistic insights into how SBF misregulation impedes transition
477 from mitotic to meiotic cell fate (Figure 6F).
478

479 **Rewiring of the G1/S regulon**

480 It has long been known that entry into the mitotic cell cycle and meiotic differentiation are
481 regulated differently. During the mitotic cell cycle, budding yeast cells must reach a critical
482 size before commitment to division in late G1 phase, an event termed the “Start” (Hartwell
483 et al., 1974; Johnston et al., 1977). Start depends on the activation of the G1/S regulon
484 by SBF and MBF, which regulate ~200 genes that function in polarized growth,
485 macromolecular biosynthesis, DNA replication, and repair among other critical processes

486 (reviewed in Jorgensen and Tyers, 2004). In contrast, entry into meiosis requires the
487 transcriptional activator, Ime1, which is exclusively induced in diploid cells through the
488 integration of several extrinsic cues including nitrogen levels, carbon source and
489 extracellular pH (reviewed in van Werven and Amon, 2011). Ime1 initiates the first
490 transcriptional wave of early meiotic genes required for DNA replication, recombination,
491 and chromosome morphogenesis. Before our study, it was unclear whether and how
492 SBF-MBF activity is regulated during the transition from mitosis to meiosis, despite the
493 transcriptome-wide differences between these two developmental programs. We found
494 that during meiotic entry, the SBF-specific Swi4 subunit is downregulated, which indicates
495 that the activity of SBF, but not MBF, is constrained. Consistently, SBF-specific targets
496 display either low or no expression during early meiosis, while MBF targets are
497 upregulated upon meiotic entry. MBF targets are involved in processes shared between
498 mitosis and meiosis including DNA replication and repair, whereas SBF targets are
499 predominantly involved in processes unique to mitosis such as budding and cell wall
500 biosynthesis. This functional specialization might have enabled adaptations to
501 accommodate specific cell fates. Likewise, SBF-specific targets that are detrimental to
502 meiosis, such as the G1 cyclins (Colomina et al., 1999, and this study), might contribute
503 to the mutually exclusive nature of the mitotic and meiotic programs.
504
505 Absolute measurements of the concentrations of SBF and MBF in single cells during
506 mitotic G1 demonstrated that these transcription factors are sub-saturating with respect
507 to their target promoters in small cells, but that SBF and MBF levels increase as cells
508 grow, suggesting that their abundance is a limiting factor in activating the G1/S regulon

509 (Dorsey et al., 2018). Corroborating these findings, we show that overexpression of *SWI4*
510 as well as the simultaneous disruption of the two pathways that normally restrict SBF
511 activity at meiotic entry – namely LUTI and Whi5 – result in abrupt activation of the SBF
512 regulon and a concomitant decrease in early meiotic gene expression. However, MBF
513 targets do not seem to be affected in response to increased SBF activity. This is surprising
514 given that SBF and MBF share a common subunit, Swi6, and that an upsurge in Swi4
515 abundance might be expected to titrate Swi6 away from MBF. It is possible that meiosis-
516 specific regulators like Ime1 and Ime2 compensate to maintain MBF target expression
517 (Brush et al., 2012). Future studies are necessary to dissect the meiotic roles of MBF and
518 potential compensatory mechanisms.
519
520 **Inhibition of G1 cyclins during meiotic entry and vice versa**
521 We found that the meiotic entry delay due to untimely SBF activation can be partially
522 rescued by loss of either *CLN1* or *CLN2*, demonstrating that both cyclins are responsible
523 for the meiotic defects associated with SBF misregulation. In addition to *CLN1* and *CLN2*,
524 improper activation of SBF also leads to upregulation of *PCL1* during meiotic entry (Figure
525 2F and 6B). *PCL1* encodes a cyclin that interacts with the Pho85 CDK and is involved in
526 the regulation of polarized cell growth and morphogenesis as well as progression through
527 the cell cycle (Espinoza et al., 2016). Whether *PCL1* misexpression contributes to the
528 SBF-associated meiotic entry defects is an interesting avenue for future studies.
529
530 We and others have demonstrated that elevated levels of G1 cyclins inhibit meiotic entry.
531 Therefore, it is crucial to dissect the mechanisms that govern the downregulation of G1

532 cyclins during this process. Among the G1 cyclins that are known to inhibit meiotic entry
533 (Colomina et al., 1999), only the mechanism of *CLN3* restriction was previously known
534 (Parviz and Heideman, 1998; Gallego et al., 1997). Our study provides a mechanistic
535 understanding of how *CLN1* and *CLN2* remain quiescent during meiotic entry through the
536 combined act of LUTI-based and Whi5-dependent inhibition of SBF. Whether additional
537 mechanisms play a role in restricting SBF and/or *CLN1*-*CLN2* remains to be determined.
538
539 Our findings also shed light on the mechanism by which G1 cyclins prevent meiotic entry.
540 Previous work demonstrated that G1 cyclin overexpression leads to downregulation of
541 *IME1* expression and inhibition of Ime1 nuclear localization (Colomina et al., 1999). Even
542 though we observed similar defects in *IME1* in response to *CLN2* overexpression,
543 increasing *IME1* expression or targeting Ime1 to the nucleus did not result in successful
544 meiosis (Figure 4). Instead, we found that restoring the interaction between Ime1 and its
545 cofactor Ume6 was sufficient to bypass the meiotic blockage exerted by Cln/CDK.
546 Collectively, our analyses suggest that the primary reason why G1 cyclins cause a meiotic
547 failure is due to a deficiency in Ime1-Ume6 interaction. A previous study reported that G1
548 cyclins do not affect the interaction between Ime1 and Ume6 (Colomina et al., 1999).
549 However, this conclusion was based on the use of a truncated Ime1 protein that only
550 contained the Ume6 interaction domain. Therefore CLN-dependent regulations on full-
551 length Ime1 might be missed in this context.
552
553

554 Future work could be aimed at dissecting how G1 cyclins affect the interaction between
555 Ime1 and Ume6 and whether their impact on Ime1's subcellular localization is primarily
556 due to G1 cyclin-dependent changes in Ime1-Ume6 interaction. Since there are no CDK
557 consensus phosphorylation sites on Ime1 itself, other players are likely to be involved.
558 Rim11 and Rim15 are potential candidates since these two kinases have been implicated
559 in Ime1-Ume6 phosphorylation as well as regulation of Ime1 localization and its
560 interaction with Ume6 (Rubin-Bejerano et al., 1996; Vidan and Mitchell, 1997; Bowdish et
561 al., 1994). Interestingly, Rim15 contains CDK consensus phosphorylation sites (Holt et
562 al., 2009; Moreno-Torres et al., 2017; Breitkreutz et al., 2010), Furthermore, Cln2/CDK
563 activity has been previously shown to inhibit Rim15 nuclear localization (Talarek et al.,
564 2010), thereby making it an attractive candidate for further investigation.
565

566 **Antagonistic relationship between two key transcription factors, Swi4 and Ime1**

567 Swi4 and Ime1 regulate each other in an antagonistic manner (Figure 6F), as supported
568 by several observations. First, overexpression of *SWI4* leads to a reduction in Ime1
569 nuclear localization (Figure 2B). Second, premature activation of SBF through *SWI4*
570 overexpression or simultaneous disruption of *SWI4*^{LUTI} and Whi5 pathways results in a
571 significant delay in the chromosomal localization of Rec8, a direct transcriptional target of
572 Ime1 (Figure 2H, 2I and 6E). Additionally, many early meiotic genes that are also
573 transcriptional targets of Ime1 are downregulated under the same conditions (Figure 2F
574 and 6D). Third, *IME1* is inhibited by the G1 cyclins, which are themselves targets of
575 Swi4/SBF (Figure 4). The reverse regulation, where Ime1 inhibits Swi4, is also in place.
576 This occurs through the Ime1-dependent expression of *SWI4* ^{LUTI}, which is necessary to

577 downregulate Swi4 levels (Figure 5, also reported in Tresenrider et al., 2021). The
578 antagonistic relationship between Swi4 and Ime1 is further evidenced by their mutually
579 exclusive pattern of nuclear localization at the single-cell level (Figure 2E). In summary,
580 our study highlights the multiple ways in which Swi4 and Ime1 regulate each other, which
581 likely plays a crucial role in cellular decision making between the mitotic and meiotic
582 transcriptional programs.
583
584 **Intersection of LUTI-based gene repression with other regulatory pathways**
585 While LUTI-based regulation is both necessary and sufficient to downregulate Swi4
586 levels, disrupting it alone is not enough to activate the SBF regulon. We found that the
587 LUTI-based mechanism works together with the Whi5 pathway to inhibit SBF activity
588 (Figure 6). As a result, only when both mechanisms are simultaneously disrupted, do cells
589 exhibit abrupt activation of SBF targets and subsequent meiotic entry defects. This two-
590 pronged inhibition of SBF activity is reminiscent of how meiotic cells prevent microtubule-
591 kinetochore interactions during prophase I (Miller et al., 2012). Specifically, LUTI-based
592 regulation represses the expression of a limiting outer kinetochore subunit, Ndc80 (Chen
593 et al., 2017). Even when the outer kinetochore assembles upon disruption of *NDC80*^{LUTI},
594 microtubules are still unable to engage with the kinetochores due to restriction of Clb/CDK
595 activity. The loss of both regulations results in meiotic chromosome segregation defects
596 (Chen et al., 2017). Integrating LUTI-based repression into larger regulatory networks
597 likely ensures robustness in cellular decision-making, providing a fail-safe system.
598 However, combinatorial use of the LUTI-based mechanism with other regulatory
599 pathways poses a challenge to uncover their functional importance. Despite 8% of the

600 yeast genes being subject to LUTI-based regulation during meiosis (Cheng et al., 2018),
601 the biological significance of only two LUTIs, *NDC80*^{LUTI} and *SWI4*^{LUTI}, have been
602 uncovered thus far. Therefore, systematic studies aiming to dissect the biological roles of
603 LUTIs in meiosis and beyond would benefit from simultaneous perturbation approaches,
604 including synthetic genetic interactions.
605

606 **Concluding remarks**

607 Cell state changes are primarily governed by transcription factors. Our study highlights
608 how transition from mitotic to meiotic cell fate is ensured by inhibition of the SBF
609 transcription factor through two distinct mechanisms. The SBF regulon includes G1
610 cyclins, whose untimely expression blocks meiotic entry by disrupting the interaction
611 between Ime1 and Ume6, a key transcriptional co-activator of meiosis. SBF and Ime1-
612 Ume6 antagonize each other, thereby helping establish a mutually exclusive state
613 between the mitotic and meiotic transcriptional programs. Mammalian cells have
614 functional homologs to both sets of transcription factors. First, similar to Ume6, MEIOSIN
615 binds to the promoters of early meiotic genes and recruits Ime1-like STRA8 to activate
616 gene expression (Anderson et al., 2008; Kojima et al., 2019; Baltus et al., 2006; Ishiguro
617 et al., 2020). Second, SBF and MBF counterparts in mammalian cells are known as E2Fs,
618 nine of which control the G1/S transition (reviewed in Van Den Heuvel and Dyson, 2008).
619 Each E2F regulates a distinct sets of genes (Gaubatz et al., 2000). Furthermore, some
620 members of the E2F family are involved in tissue-specific regulation of cell fate (Julian et
621 al., 2016). However, the molecular mechanisms driving the rewiring of these complex
622 gene networks are not well understood. Our investigation could help shed light on the

623 regulatory mechanisms governing the interplay between mitotic and meiotic transcription
624 factors outside of yeast.
625
626 **MATERIALS AND METHODS**
627
628 **Strain Construction and Cloning**
629 All strains used in this study were derived from the SK1 background. Detailed information
630 about the strain genotypes can be found in Supplemental Table 4.
631
632 For *SWI4* (pUB1587) 1200 bases upstream of the ORF, *SWI4* ORF, C-terminal 3V5
633 epitope tag, and *SWI4* 3'UTR (1000 bases downstream of ORF) were cloned into a *LEU2*
634 single integration vector by Gibson assembly (NEB) (Gibson et al., 2009). LUTI promoter
635 deletion (Δ*LUTI*) strain (pUB1588) was similarly constructed with -1200 to -934 bases
636 upstream from ORF deleted. For the uORF mutant (Δ*uORF*) strain (pUB1734) all seven
637 ATG uORFs were mutated using gBlocks with the ATG>ATC mutations and cloned by
638 Gibson assembly into 3V5-tagged *LEU2* single integration vector. In all strains described
639 above, the endogenous *SWI4* gene is deleted using Pringle-based insertion of KanMX6
640 marker (Bähler et al., 1998).
641
642 For overexpression of *SWI4 (pUB1585)*, *CLN1 (pUB2144)*, and *CLN2 (pUB1899)*, the
643 relevant gene carrying a 3V5 epitope tag was cloned downstream of the *ATG8* promoter,
644 which is highly expressed during meiosis (Brar et al., 2012). A *LEU2* single integration
645 vector was used for cloning the fragments by Gibson assembly (*NEB*). In the strains
646 carrying overexpression transgenes, the wild-type alleles at the endogenous loci
647 remained intact. *pCUP1-GFP-IME1* allele was made with Pringle-based insertion of the
648 *pCUP1* promoter upstream of *GFP-IME1*. *PUS1*-αGFP and *UME6*-αGFP were made by
649 Pringle-based insertion using a plasmid (pUB1707) gifted by the Lackner Lab. For *WHI5-*
650 *AA* the *WHI5-mCherry-FRB* allele was made by Pringle-based insertion using a plasmid
651 (pUB595) gifted by the Nasmyth lab. All plasmid sequences were confirmed by
652 sequencing.

653

654 All single integration plasmids were digested with Pme1 before transformation. Proper
655 integration was confirmed by PCR. The plasmids constructed in this study are listed in
656 Supplemental Table 5.

657

658 **Sporulation Conditions**

659 For meiotic experiments using *pCUP1-IME1/pCUP1-IME4* or *pCUP-IME1* system, cells
660 were synchronized as described in (Chia and van Werven, 2016). Briefly, after 24 h of
661 growth in YPD at room temperature, saturated cultures (OD_{600} > 10) were diluted to an
662 OD_{600} of 0.25 in BYTA (1% yeast extract, 2% bacto tryptone, 1% potassium acetate, and
663 1.02% potassium phthalate) for 16-18 h of growth at 30°C (OD_{600} of > 5). Cells were
664 washed with water twice before final resuspension in SPO with 0.5% potassium acetate
665 to an OD_{600} of 1.85. After 2 h in SPO, *IME1* and *IME4* were induced with 50 μM $CuSO_4$.
666 Sporulation efficiency was measured after 24 h in SPO. Anchor away meiotic experiments
667 was performed as described above with final 1 μM rapamycin (Millipore) added to BYTA
668 30 minutes before transfer to SPO and again 1 μM rapamycin added to SPO media.

669

670 In all other meiotic experiments, cells were prepared as in (Carlile and Amon, 2008).
671 Briefly, after 24 h of growth in YPD at room temperature, saturated cultures (OD_{600} > 10)
672 were diluted to an OD_{600} of 0.25 and inoculated in BYTA (1% yeast extract, 2% bacto
673 tryptone, 1% potassium acetate, and 1.02% potassium phthalate) for 16-18 h at 30°C
674 (OD_{600} of > 5). Cells were washed with water twice before final resuspension in SPO with
675 0.5% potassium acetate to an OD_{600} of 1.85. Sporulation efficiency was counted after 24
676 h in SPO.

677

678 *UME6-αGFP* meiotic experiments were prepared as in (Chia and van Werven, 2016).
679 Briefly, after 18 h of growth in YPD at room temperature, saturated cultures (OD_{600} > 10)
680 were diluted to an OD_{600} of 0.2 in reduced YPD (1% yeast extract, 2% peptone, 2%
681 dextrose, uracil [24 mg/L]). Reduced YPD was used instead of BYTA to prevent cells from
682 prematurely entering meiosis in BYTA due to the Ime1-Ume6 interaction from the GFP
683 nanobody. Cells were grown for ~6 h at 30°C until they reached an OD_{600} between 0.5

684 and 1.0. Cultures were then back diluted to OD_{600} of 0.1 and grown for 18 h at 30°C. Cells
685 were washed with water twice before final resuspension in SPO with 0.5% potassium
686 acetate to an OD_{600} of 1.85. Sporulation efficiency was counted after 24 h in SPO.
687
688 **RNA Extraction for mRNA-seq, RT-qPCR, and RNA Blotting**
689 RNA extraction was performed as described in (Tresenrider et al., 2021). Briefly, ~4
690 OD unit of cells were pelleted by centrifugation for 1 minute at 20,000 rcf and snap frozen
691 in liquid nitrogen. Cells were thawed on ice and resuspended in TES buffer (10 mM Tris
692 pH 7.5, 10 mM EDTA, 0.5% SDS). An equal volume of Acid Phenol:Chloroform:Isoamyl
693 alcohol (125:24:1; pH 4.7) was added to cells and incubated at 65°C for 45 min shaking
694 at 1400 rpm. Aqueous phase was transferred to a new tube with chloroform, vortexed for
695 30 sec, separated by centrifugation, and precipitated in isopropanol and sodium acetate
696 overnight at -20°C. Pellets were washed with 80% ethanol and resuspended in DEPC
697 water for 10 min at 37°C. Total RNA was quantified using a nanodrop.
698
699 **mRNA Sequencing (mRNA-seq) and Analysis**
700 RNA-seq libraries were generated with the NEXTflex™ Rapid Directional mRNA-Seq Kit
701 (NOVA-5138, Perkin Elmer). 10 µg of total RNA was used as input for all
702 libraries. AMPure XP beads (A63881, Beckman Coulter) were used to select fragments
703 between 200-500 bp. Libraries were quantified using the Agilent
704 4200 TapeStation (Agilent Technologies, Inc). Samples were submitted for 100 bp SE
705 sequencing by the Vincent J. Coates Genomics Sequencing Laboratory with a NovaSeq
706 SP 100SR.
707
708 Hisat2 (Kim et al., 2019) was used to align reads to map sequences to SK1 PacBio
709 genome. Quantification of RNA as transcripts per million was done StringTie (Pertea et
710 al., 2015). Fold-change quantification was performed by DESeq2 using default options
711 (version 1.34.0, (Love et al., 2014)).
712
713 For Gene Set Enrichment Analysis (GSEA) v4.3.2 was used to compare TPM values for
714 different gene sets. The early meiotic gene set was created from Figure 2 of (Brar et al.,

715 2012). The SBF regulon was from Figure 3 of (Iyer et al., 2001). GSEA was performed
716 on the desktop app with default settings expect “Collapse/Remap to gene symbols” was
717 set to “No_Collapse” and “Permutation type" was set to "gene_set”.
718
719 For Gene Ontology (GO) Analysis, SGD Gene Ontology Slim Term Mapper was used for
720 GO analysis using Yeast Go-Slim: process GO Set. Used output from DE-Seq2 analysis
721 with a cutoff of padj (P value) < 0.05.
722
723 The two overlapping targets (*SWE1* and *TOS4*) between the early meiotic gene set and
724 SBF targets are not plotted on volcano plot or used for GSEA analysis.
725
726 **Reverse Transcription-Quantitative Polymerase Chain Reaction (RT-qPCR)**
727 5 μg of isolated total RNA was treated with DNase (TURBO DNA-free™ Kit). cDNA was
728 reverse transcribed following the Superscript III kit (ThermoFisher Scientific).
729 Quantification was performed with Absolute Blue qPCR Mix (ThermoFisher Scientific).
730 Meiotic samples were normalized to *PFY1,* and mitotic samples were normalized to
731 *ACT1.* Oligonucleotides are listed in Supplemental Table 6.
732
733 **Protein Extraction and Immunoblotting**
734 ~4 OD_{600} of cells were collected and pelleted by centrifugation for 1 min at 20,000 rcf.
735 Pellet was resuspended in 5% (w/v) TCA for at least 15 min at 4°C. Cells were washed
736 with TE50 (50 mM Tris-HCl [pH 7.5], 1 mM EDTA) and then with 100% acetone. The cell
737 pellet was dried overnight and then lysed with glass beads in lysis buffer (Tris-HCl [pH
738 7.5], 1 mM EDTA, 2.75 mM DTT, protease inhibitor cocktail (cOmplete EDTA-free
739 [Roche]). Next 3x SDS sample buffer (187.5 mM Tris [pH 6.8], 6% β-mercaptoethanol,
740 30% glycerol, 9% SDS, 0.05% bromophenol blue) was added and the cell lysate was
741 boiled for 5 min at 95°C. Protein was separated by PAGE using 4-12% Bis-Tris Bolt gels
742 (Thermo Fisher) and transferred onto 0.45 µm nitrocellulose membranes.
743
744 Cln1-3V5, Cln2-3V5 and GFP-GFP tagged proteins were all transferred onto 0.45 µm
745 nitrocellulose membranes using a semi-dry transfer apparatus (Trans-Blot Turbo System

746 (Bio-rad)). Swi4-3V5 or untagged Swi4, Swi6, and Mbp1 proteins were all transferred onto
747 0.45 µm nitrocellulose membranes using a PROTEAN Tetra tank (BioRAD) filled with 25
748 mM Tris, 192 mM glycine, and 7.5% methanol. All blots were incubated at room
749 temperature with Odyssey Blocking Buffer (PBS) (LI-COR Biosciences).
750
751 Immunoblotting for Cln1-3V5, Cln2-3V5, and GFP-Ime1 was performed as previously
752 described in (Tresenrider et al., 2021). Briefly, mouse α-V5 antibody (R960-25, Thermo
753 Fisher) or mouse α-GFP antibody (632381, Takara) were diluted 1:2000 in Odyssey
754 Blocking Buffer (PBS) (LI-COR Biosciences) with 0.01% Tween. Rabbit α-hexokinase (α-
755 Hxk2) antibody (H2035, US Biological) was diluted to 1:20,000. Secondary antibodies
756 used were α-mouse antibody conjugated to IRDye 800CW (926-32212, LI-COR
757 Biosciences) and α-rabbit antibody conjugated to IRDye 680RD (926-68071, LI-COR
758 Biosciences). Secondary antibodies were diluted to 1:20,000 in Odyssey Blocking Buffer
759 (PBS) with 0.01% Tween.
760
761 For immunoblotting of Swi4, Swi6, and Mbp1. antibodies specific to each subunit were a
762 generous gift from the Andrews and deBruin labs (Andrews and Herskowitz, 1989; Harris
763 et al., 2013). α-Swi4, α-Swi6, α-Mbp1 antibodies were each diluted to 1:2000 in Odyssey
764 Blocking Buffer (PBS) (LI-COR Biosciences) with 0.01% Tween. Secondary antibodies
765 included a α-rabbit antibody conjugated to IRDye 800CW (926-32213, LI-COR
766 Biosciences) and a α-rabbit antibody conjugated to IRDye 680RD (926-68071, LI-COR
767 Biosciences).
768
769 Odyssey system (LI-COR Biosciences) was used to image the blots, and Image Studio
770 Lite (LI-COR Biosciences) was used for image quantification.
771
772 **Northern (RNA) Blotting**
773 For each blot, 10 µg of total RNA was dried in a Savant Speed Vac (SPD111V). RNA was
774 then resuspended and denatured in glyoxal/DMSO mix (1M deionized glyoxal, 50% v/v
775 DMSO, 10 mM sodium phosphate (NaPi) buffer [pH 6.8]) at 70°C for 10 min. RNA sample
776 was loaded into an agarose gel (1.1% [w/v] agarose in 0.01 M NaPi buffer) with loading

777 dye (10% v/v glycerol, 2 mM NaPi buffer [pH 6.8], ~0.25% w/v xylene cyanol, and orange
778 G) and ran for 3 h at 100 V with a Variable Speed Pump (BioRad) to circulate buffer during
779 the entire gel run.
780
781 RNA was transferred overnight to nylon membrane (Hybond-N+ [GE]) in SSC. Membrane
782 was crosslinked using a Stratalinker UV Crosslinker (Stratagene). Ribosomal RNA
783 (rRNA) bands were visualized with methylene blue staining and imaged on a Gel Doc
784 XR+ Molecular Imager with Image Lab software (BioRad).
785
786 Probe templates containing the T7 promoter were amplified using PCR. PCR product was
787 concentrated with MinElute Spin Columns (Qiagen) and then used for *in vitro* transcription
788 to generate a strand-specific RNA probe using a MaxiScript T7 Kit (Invitrogen) according
789 to the manufacturer's instructions, except cold UTP was replaced with α-P32 labeled UTP
790 (PerkinElmer). Excess nucleotides were removed with NucAway Spin Columns
791 (Invitrogen). Blots were blocked in ULTRAhyb Ultrasensitive Hybridization Buffer
792 (Invitrogen) for 1 h and then incubated with the α-P32 labeled probe overnight at 68°C.
793 Blots were then washed twice with low stringency wash buffer (2X SSC, 0.1% SDS) for
794 10 min and then washed twice with high stringency wash buffer (0.1X SSC, 0.1% SDS)
795 for 15 min. Blots were then exposed overnight on a storage phosphor screen (Molecular
796 Dynamics) and then imaged on a Typhoon phosphor-imaging system.
797
798 **Fluorescence Microscopy**
799 For time course imaging of cells expressing *GFP-IME1*, *SWI4-mCherry*, or *WHI5-*
800 *mCherry*, 500 µL of meiotic culture was fixed with a final concentration of 3.7%
801 formaldehyde (v/v) at room temperature for 15 min. Cells were then washed in 1 ml of
802 100 mM potassium phosphate [pH 6.4] and stored at 4°C in 20 µl of KPi Sorbitol solution
803 overnight (100 mM potassium phosphate [pH 7.5], 1.2M sorbitol). Cells were mounted on
804 a slide and imaged using DeltaVision Elite wide-field fluorescence microscope (GE
805 Healthcare) with a 60x/1.516 oil immersion objective. Deconvolution of images was done
806 with softWoRx imaging software (GE Life Sciences).
807

808 For live-cell imaging, cells at OD_{600} of 1.85 in conditioned SPO (filter-sterilized SPO
809 culture after ~5 h in 30°C) were sonicated and transferred to a concanavalin A (Sigma)
810 treated 96-well clear, flat bottom plate (Corning). Four z positions (2 µm step size) were
811 acquired per XY position. Acquisition was performed in a temperature-controlled chamber
812 at 30°C. Please refer to Supplemental Table 7 for acquisition settings.
813
814 **Image Quantification**
815 All image analysis was performed with FIJI (Schindelin et al., 2012). Maximum z-
816 projection are shown in figures and were modified using linear brightness and contrast
817 adjustments in FIJI.
818
819 To quantify localization of GFP-Ime1 and Rec8-GFP, z-slices containing the nucleus were
820 selected using the Htb1-mCherry signal. Max projection was created from these slices
821 and GFP-Ime1 was scored double-blinded as nuclear or not nuclear.
822
823 For mean nuclear intensity of GFP-Ime1 and Swi4-mCherry, an individual z-slice
824 containing the nucleus was selected and nuclear mask was generated using the Htb1-
825 mCherry signal. The nuclear mask was then used to quantify the mean nuclear intensity
826 of GFP-Ime1 signal.
827
828 **Single molecule RNA FISH**
829 smFISH was performed and quantified as previously described in (Chen et al., 2018). All
830 probes were ordered from (Biosearch Technologies). Unique region of $SWI4^{LUTI}$ was
831 visualized by twenty-eight 20-mer oligonucleotide probes coupled to CAL fluor Red 590.
832 Thirty-eight 20-mer probes coupled to Quasar 670 dye targeted to $SWI4^{canon}$. ~ 4 OD unit
833 of cells were fixed in final 3% formaldehyde (v/v) and incubated at room temperature for
834 20 minutes. Fixed samples were moved to 4°C to continue fixing overnight. Cells were
835 washed three times in cold Buffer B (0.1 M potassium phosphate [pH 7.5], 1.2 M sorbitol)
836 and resuspended in digestion buffer (Buffer B, 200 mM Vanadyl ribonucleoside complex
837 [VRC from NEB], zymolyse [zymolase 100T, MP Biomedicals]). Cells were digested at

838 30°C for 20 min and then gently washed with 1 mL of cold Buffer B and resuspended in
839 1 mL of 70% ethanol for 3.5-5 h.
840
841 Cells were then incubated in 1mL of 10% formamide wash buffer (10% formamide, 2X
842 SSC) at room temperature for 15 minutes. For hybridization, each probe set was added
843 (final concentration of 500 nM) to 20mM VRC and hybridization buffer (1% Dextran sulfate
844 [EMD Millipore], 1 mg/mL E. coli tRNA [Sigma], 2 mM VRC, 0.2 mg/mL BSA, 1X SSC,
845 10% formamide in nuclease-free water). Hybridization was done overnight at 30°C.
846 Samples were incubated in the dark for 30 min at 30°C in 1 mL of 10% formamide wash
847 buffer. Buffer was then removed, and cells were stained with DAPI and resuspended in
848 glucose-oxygen-scavenging buffer or GLOX buffer (10 mM Tris [pH 8.0], 2x SSC, 0.4%
849 glucose) without enzymes. Before imaging, GLOX solution with enzyme (1% v/v catalase,
850 1% v/v glucose oxidase (Sigma), 2 mM Trolox (Sigma)) was added to sample.
851
852 Images were acquired with the DeltaVision microscope as described in previous section
853 with filters: TRITC (EX542/27, EM597/45) for CAL Fluor Red 590 and CY5 (EX632/22,
854 EM679/34) for Quasar 670. Series of z-stacks (15–25 slices) were acquired with a step
855 size of 0.2 μm.
856
857 Matlab script (Chen et al., 2017, 2018) was run to quantify FISH spots with max intensity
858 projection of z-stacks. The same "signal" and "SNR" thresholds were applied to all the
859 images within a replicate.
860
861 **Resource availability**
862 All materials used in this study are available upon request from the corresponding author.
863 Sequencing data generated in this study are available at NCBI GEO under the accession
864 ID: GSE225963
865 The custom code used for the analysis is available in the following code repository:
866 https://github.com/elifesciences-publications/Chen_Tresenrider_et_al_2017

Acknowledgements:

We thank Gloria Brar, Nick Ingolia, Rebecca Heald, Kathlyeen Ryan, Jingxun Chen, Anthony Harris, Andrea Higdon, Grant King, Jessica Leslie, Kate Morse, Emily Powers, Cyrus Ruediger, Tina Sing, and Ben Styler for suggestions and comments on this manuscript, David McSwiggen and Yuichiro Iwamoto for technical support, all members of the Ünal and Brar labs and Jeremy Thorner for valuable discussions. This work is supported by funds from the National Institutes of Health (R01 GM140005) and Astera Institute to E.Ü. and a National Institutes of Health Traineeship (T32 GM007232) to A.J.S.

Author contributions:

A.J.S, conceptualization, data curation, formal analysis, investigation, methodology, validation, visualization, and drafting of the manuscript. S.C.Y, data curation, formal analysis, investigation, methodology, validation, visualization. E.Ü., conceptualization, methodology, visualization, supervision, project administration, funding acquisition, and drafting of the manuscript.

Figure Legends

Figure 1. Swi4 subunit of the SBF and SBF targets are downregulated during early meiosis

A. A schematic of SBF and MBF complexes and the general functional groups of the genes they regulate. **B.** Samples from strain UB35246 were collected between 0-6 hours (h) in sporulation medium (SPO) and immunoblots were performed using α-Swi4, α-Swi6, and α-Mbp1 respectively. Hxk2 was used a loading control. Representative blots from one of two biological replicates are shown. **C.** Quantification of the immunoblots in (B). The signal at each time point was first normalized to Hxk2 loading control and then to the

892 max signal. **D.** Scatterplot of RNA-seq data (RPKM) from (Brar et al., 2012) comparing 2
893 h in SPO vs. mitotic growth of well characterized SBF targets (pink) and MBF targets
894 (teal). **E.** Wild type (UB22199) and *pATG8-SWI4* (UB22226) cells were collected to
895 perform RT-qPCR for *CLN1, CLN2, CDC21,* and *RNR1* transcripts. Transcript abundance
896 was quantified using primer sets specific for each respective gene from three technical
897 replicates for each biological replicate. Quantification was performed in reference to *PFY1*
898 and then normalized to wild-type control. FC = fold change. Experiments were performed
899 twice using biological replicates, mean value plotted with range. Differences in wild type
900 versus *pATG8-SWI4* transcript levels at 2 h in SPO compared with a two-tailed t-test (*,
901 p = 0.0351 [*CLN1*]; **, p = 0.0013 [*CLN2*]; ns, p = 0.8488 [*CDC21*]; ns, p = 0.0859
902 [*RNR1*]). **F.** Live-cell imaging of strains containing the fluorescently tagged histone Htb1-
903 mCherry for wild type (UB32085) and *pATG8-SWI4* (UB32089). Experiments were
904 performed twice using biological replicates, mean value plotted with range. Differences in
905 meiotic progression tested by Mann Whitney test, two-tailed (**, p = 0.0045).
906

907 **Figure 2. Regulation of Swi4 abundance is required for timely meiotic entry**

908 **A-B.** Fixed imaging of cells marked with GFP-Ime1 and Htb1-mCherry. Wild type
909 (UB22199) and *pATG8-SWI4* (UB22226) cells were collected between 0-4 h in SPO. **A.**
910 Representative images with merge at 0 h and 2 h in SPO. Representative cells outlined.
911 Scale bar: 3 µm. **B.** Quantification as percent cells with nuclear Ime1. Experiments were
912 performed twice using biological replicates, mean value plotted with range. Total of 200
913 cells analyzed per strain. Differences in the fraction of cells with nuclear Ime1 was
914 compared using a two- tailed t-test (**, p = 0.0099 [1 h in SPO]; *, p = 0.0169 [2 h in SPO];

915 *, p = 0.0315 [3 h in SPO]; ns, two-tailed p = 0.4595 [4 h in SPO]). **C-E.** Fixed imaging of
916 cells marked with GFP-Ime1 and Swi4-mCherry. Wild type (UB31378) and *pATG8-SWI4*
917 (UB31381) cells were collected at 0 h and 4 h in SPO. **C.** Example images with merge at
918 4 h in SPO. Example cells outlined (*low nuclear GFP-Ime1 with high nuclear Swi4-
919 mCherry, **high nuclear GFP-Ime1 with low nuclear Swi4-mCherry). Scale bar: 3 µm. **D.**
920 Scatterplot of GFP-Ime1 mean nuclear intensity and Swi4-mCherry mean nuclear
921 intensity for wild type and *pATG8-SWI4* cells at 0 h in SPO. See Materials and Methods
922 for further details about image quantification. Dashed line is linear regression plotted for
923 each condition and strain. A total number of 269 cells were analyzed. **E.** Same as in (D)
924 but for wild type and. *pATG8-SWI4* cells at 4 h in SPO. A total number of 341 cells were
925 analyzed. Differences in mean nuclear GFP-Ime1 or Swi4-mCherry intensity between wild
926 type and *pATG8-SWI4* compared using a Mann-Whitney test, two-tailed (****, p < 0.0001
927 [wild type vs. *pATG8-SWI4* (GFP-Ime1)]; ****, p < 0.0001 [wild type vs. *pATG8-SWI4*
928 (Swi4-mCherry)]). **F.** Volcano plot of DE-Seq2 analysis for *pATG8-SWI4* versus wild type.
929 Dashed line indicates padj (p value) = 0.05. Analysis was performed using mRNA-seq
930 from two biological replicates. Wild type (UB22199) and *pATG8-SWI4* (UB22226) cells
931 were collected at 2 h in SPO. SBF targets (pink) (Iyer et al., 2001) and early meiotic genes
932 (blue) defined by (Brar et al., 2012). Darker pink or darker blue, labeled dots are well
933 studied targets in either gene set list. **G.** GSEA analysis of mRNA-seq comparing wild
934 type vs. *pATG8-SWI4* collected at 2 h in SPO. Vertical black bars represent the early
935 meiotic cluster from (Brar et al., 2012) or SBF cluster from (Iyer et al., 2001). The heatmap
936 indicates genes that are more enriched in *pATG8-SWI4* (red, left-side) or genes that are
937 enriched in wild type (blue, right-side). NES = normalized enrichment score. Enrichment

938 was determined by comparing *pATG8-SWI4* versus wild type. **H-I.** Live-cell imaging of
939 cells in meiosis marked by Rec8-GFP and nuclear marker Htb1-mCherry for wild type
940 (UB32085) and *pATG8-SWI4* (UB32089). **H.** Movie montage with example images
941 throughout meiosis for Rec8-GFP and Htb1-mCherry. Scale bar: 3 μm **I.** Quantification
942 as percent of cells that entered meiosis assayed by nuclear Rec8 appearance.
943 Experiments were performed using two biological replicates, mean value plotted with
944 range. A total number of 452 cells were analyzed. Differences in meiotic progression
945 compared by Mann Whitney test, two-tailed (***, p = 0.0005 [wild type vs. *pATG8-SWI4*]).
946

947 **Figure 3. Removal of the SBF targets Cln1 or Cln2 partially rescues the meiotic**
948 **entry delay in the *pATG8-SWI4* mutant**

949 **A.** Immunoblotting was performed on samples collected for wild type (UB29326) and
950 *pATG8-SWI4* (UB29328) between 0-6 h in SPO using α-V5 antibody to track Cln1-3V5.
951 Hxk2 was used a loading control. Representative blots from one of two biological
952 replicates are shown. **B.** Quantification of (A). **C.** Same as in (A) but for wild type
953 (UB29330) and *pATG8-SWI4* (UB29332) cells using α-V5 antibody to track Cln2-3V5.
954 Hxk2 was used a loading control. Representative blots from one of two biological
955 replicates are shown. **D.** Quantification of (C). **E.** Live-cell imaging of meiotic cells marked
956 by Rec8-GFP and nuclear marker Htb1-mCherry, with the following genotypes: wild type
957 (UB32085), *pATG8-SWI4* (UB32089), and *pATG8-SWI4*; *cln1*Δ (UB34536).
958 Quantification of cells that entered meiosis assayed by the initial timing of nuclear Rec8
959 appearance. Experiments were performed using two biological replicates, mean value
960 plotted with range. A total number of 883 cells were analyzed. Differences in meiotic

961 progression compared by Mann-Whitney test, two-tailed (*, p = 0.0111 [*pATG8-SWI4* vs.
962 *pATG8-SWI4*; *cln1*Δ]). *cln1*Δ alone (not shown) has similar meiotic progression kinetics
963 relative to wild type. **F.** Same as (E) but with the following genotypes: wild type
964 (UB32085), *pATG8-SWI4* (UB32089), and *pATG8-SWI4*; *cln2*Δ (UB34165). A total
965 number of 610 cells were analyzed. Differences in meiotic progression compared by
966 Mann-Whitney test, two-tailed (*, p = 0.0478 [*pATG8-SWI4* vs. *pATG8-SWI4*; *cln2*Δ]).
967 *cln2*Δ alone (not shown) has similar meiotic progression kinetics relative to wild type.
968

969 **Figure 4. Tethering of Ime1 to Ume6 is sufficient to overcome the meiotic block**
970 **exerted by G1 cyclin overexpression**

971 **A.** Sporulation efficiency of cells at 24 h in SPO media wild type (UB22199), *pATG8-*
972 *CLN1* (UB32820), *pATG8-CLN2* (UB25959), *pCUP-GFP-IME1* (UB34641), *pCUP1-GFP-*
973 *IME1; pATG8-CLN2* (UB35057), *PUS1-αGFP* (UB35593), *PUS1-αGFP; pATG8-CLN2*
974 (UB35982), *UME6-αGFP* (UB35300), and *UME6-αGFP; pATG8-CLN2* (UB35177).
975 Experiments shown in this figure were performed using two biological replicates, mean
976 value plotted with range. Total of 200 cells counted per strain. See Supplementary Table
977 2 for statistics. **B-C.** Fixed imaging of cells marked with GFP-Ime1 and Htb1-mCherry.
978 Wild type (UB22199) and *pATG8-CLN2* (UB25959) cells were collected between 0-3 h in
979 SPO. **B.** Representative images with merge at 2 h in SPO. Representative cells outlined.
980 Scale bar: 3 μm. **C.** Quantification of cells with nuclear Ime1. Experiments were performed
981 using two biological replicates, mean value plotted with range. Total of 200 cells analyzed
982 per strain. Differences in percent of cells with nuclear Ime1 was compared by two-tailed
983 t-test (**, p = 0.00917 [1 h in SPO]; **, p = 0.0044 [2 h in SPO]; *, p = 0.0122 [3 h in SPO]).

984 **D.** Schematic depicting use of *pCUP1* promoter (*pCUP1-GFP-IME1*) to rescue Ime1
985 transcript and protein levels. **E-F** Fixed imaging of cells marked with GFP-Ime1 and Htb1-
986 mCherry. Cells with the following genotypes were collected at 2 h in SPO: wild type
987 (UB22199), *pATG8-CLN2* (UB35106), *pCUP1-GFP-IME1* (UB34641), and *pCUP1-GFP-*
988 *IME1; pATG8-CLN2* (UB35057). **E.** Representative images with merge and
989 representative cells outlined. Scale bar: 3 μm. **F.** GFP-Ime1 mean nuclear intensity
990 measured for a single z-slice. A total number of 433 cells were analyzed. Differences in
991 mean nuclear intensity compared by Mann-Whitney test, two tailed, (****, $p < 0.0001$
992 [*pCUP1-IME1* vs. *pCUP1-IME1; pATG8-CLN2*]). **G.** Schematic of nanobody trap strategy
993 with *PUS1-αGFP* and GFP-Ime1 to rescue Ime1 nuclear localization in meiosis. **H-I.** Fixed
994 imaging of cells marked with GFP-Ime1 and Htb1-mCherry. Cells with the following
995 genotypes were collected at 2 h in SPO: wild type (UB22199), *pATG8-CLN2* (UB35106),
996 *PUS1-αGFP* (UB35593), and *PUS1-αGFP; pATG8-CLN2* (UB35982). **H.** Representative
997 images with merge and example cells outlined. Scale bar: 3 μm. **I.** GFP-Ime1 mean
998 nuclear intensity measured for a single z-slice. A total number of 934 cells were analyzed.
999 Differences in mean nuclear intensity compared by Mann-Whitney test, two-tailed, (****,
1000 $p < 0.0001$ [wild type vs. *pATG8-CLN2*]; not significant (ns), $p = 0.6563$ [*PUS1-αGFP* vs.
1001 *pATG8-CLN2; PUS1-αGFP*]; not significant (ns), $p = 0.8881$ [wildtype vs. *pATG8-CLN2;*
1002 *PUS1-αGFP]*). **J.** Schematic of nanobody trap strategy with *UME6-αGFP* and GFP-Ime1
1003 to rescue Ime1-Ume6 interaction in meiosis. **K-L** Fixed imaging of cells marked with GFP-
1004 Ime1 and Htb1-mCherry. Cells with the following genotypes were collected at 2 h in SPO:
1005 wild type (UB22199), *pATG8-SWI4* (UB35106), *UME6-αGFP* (UB35300), and *UME6-*
1006 *αGFP; pATG8-CLN2* (UB35177). **K.** Representative images with merge and

1007 representative cells outlined. Scale bar: 3 μm. **L.** GFP-Ime1 mean nuclear intensity
1008 measured for a single z-slice. A total number of 1220 cells were analyzed. Differences in
1009 mean nuclear intensity compared by Mann-Whitney test, two-tailed (****, $p < 0.0001$ [wild
1010 type vs. *pATG8-CLN2]*; ****, $p < 0.0001$ [*UME6-αGFP* vs. *pATG8-CLN2; UME6-αGFP*];
1011 *, $p = 0.0354$ [wildtype vs. *pATG8-CLN2; UME6-αGFP*]).
1012
1013 **Figure 5. Ime1-dependent expression of a LUTI from the *SWI4* locus leads to a**
1014 **reduction in Swi4 protein levels during meiotic entry**
1015 **A.** Genome browser views of RNA-seq data (Brar et al., 2012) of the *SWI4* locus. $SWI4^{LUTI}$
1016 transcription start site is ~1045bp upstream of *SWI4* ORF translation start site. **B.** A
1017 schematic of LUTI-based gene regulation. Top: Mitotic growth, $SWI4^{LUTI}$ is repressed due
1018 to Ume6-Rpd3-Sin3 complex and $SWI4^{canon}$ is induced by one or more transcription
1019 factors including Ace2, Mbp1 and Swi5, leading to Swi4 protein production. Bottom:
1020 Meiosis-specific expression of $SWI4^{LUTI}$ by Ime1-Ume6 leads to downregulation of Swi4
1021 protein production due to combined effect of transcriptional and translation interference.
1022 $SWI4^{LUTI}$ 5′ leader contains 7 AUG uORFs but only one is shown in the model for
1023 simplicity. Schematic is adapted from (Tresenrider et al., 2021). **C.** Representative
1024 smFISH images collected from premeiotic and meiotic cells for detecting $SWI4^{canon}$ and
1025 $SWI4^{LUTI}$. Cells with *pCUP1-IME1/pCUP1-IME4* meiotic synchronization system were
1026 induced to enter meiosis with 50 μM $CuSO_4$ after 2 h in SPO. Premeiotic cells were
1027 collected before *IME1/4* induction and meiotic cells were collected 2 h post *IME1/4*
1028 induction from strain UB14273. Q 670 probes (green) hybridize to shared region within
1029 *SWI4* CDS. CF590 probes hybridize to the unique 5′ leader region of $SWI4^{LUTI}$ (depicted

1030 on the schematic shown above the images). DNA was stained with DAPI. Scale bar: 3
1031 µm. **D.** Quantification of smFISH shown in (C), plotted as relative frequency histograms
1032 of cells with *SWI4*^{canon} and *SWI4*^{LUTI} transcripts per cell. Data pooled from two
1033 independent biological replicates. Dashed line indicates median number of transcripts per
1034 cell. Each histogram is normalized with maximum bin height being the same across all
1035 histograms. A total number of 44 cells counted for premeiotic and 102 cells counted in
1036 meiotic prophase. Differences in premeiotic versus meiotic were compared by Mann-
1037 Whitney test, two-tailed (***, $p = 0.0007$ [*SWI4*^{canon}]; ****, $p < 0.0001$ [*SWI4*^{LUTI}]). **E.** RNA
1038 blot performed on cells collected between 0-6 h in SPO. All strains carry a *SWI4-3V5*
1039 tagged allele. Probe was specific for 3V5. Methylene blue staining of rRNA bands was
1040 used as a loading control. Matched immunoblotting was performed against Swi4-3V5
1041 using α-V5 and normalized to Hxk2 loading control for each sample. Cells collected are
1042 wild type (UB22199) and Δ*LUTI* (UB23012). Representative blots from one of two
1043 biological replicates are shown. **F.** Quantification of immunoblot in (E). **G.** Performed as
1044 described in (E) for wild type (UB21386) and Δ*uORF* (UB23636) strains. Representative
1045 blots from one of two biological replicates are shown. **H.** Quantification of immunoblot in
1046 (G). **I.** Immunoblot using α-V5 performed on cells collected between 0-7 h in SPO from a
1047 strain carrying *pCUP1-IME1* and *SWI4-3V5* alleles (UB34641). Swi4-3V5 abundance was
1048 normalized to Hxk2 loading control. Cells were induced to enter meiosis with 50 µM
1049 $CuSO_4$ after 2 h preincubation in SPO. Representative blots from one of two biological
1050 replicates are shown. **J.** Quantification of immunoblot in (I). **K.** Genome browser view of
1051 Ume6-ChIP at the *SWI4* locus (adapted from Tresenrider et al., 2021).
1052

1053 **Figure 6. *SWI4^{LUTI}* is integrated into a larger regulatory network to regulate SBF**
1054 **activity during meiotic entry**

1055 **A.** Volcano plot of DESeq2 analysis for Δ*LUTI* versus wild type. Dashed line indicates
1056 padj (p-value) = 0.05. Analysis was performed with mRNA-seq in duplicate. Wild type
1057 (UB27083) and Δ*LUTI* (UB26874) collected at 2 h in SPO. SBF targets (pink) and early
1058 meiotic genes (blue) defined by (Iyer et al., 2001 and; Brar et al., 2012). Darker pink or
1059 darker blue, labeled dots are well studied targets in either gene set list. **B.** Top: Schematic
1060 of the anchor-away system using *WHI5-mCherry-FRB* (*WHI5-AA*) and *RPL13a-FKBP12*
1061 alleles. Bottom: Fixed imaging of cells marked with *WHI5-mCherry-FRB* (*WHI5-AA*) with
1062 DNA stained with DAPI. 1 μM rapamycin added at 0 h in SPO to induce nuclear exclusion
1063 of Whi5 (UB25431) strain collected at 0.5 h in SPO. Scale bar: 3 μm. Cells are rapamycin
1064 resistant due to mutated *TOR1* (*tor1-1*) and frp1Δ (yeast FKBP12 homolog) to reduce
1065 competition between for binding of Frb and Fkbp12. **C.** Same as in (A) but for wild type
1066 (UB27083) and *WHI5-AA* (UB25431) collected at 2 h in SPO. **D.** Same as in (A) but for
1067 wild type (UB27083) and Δ*LUTI; WHI5-AA* (UB25428) collected at 2 h in SPO. **E.** Live-
1068 cell imaging of cells in meiosis marked by Rec8-GFP and nuclear marker Htb1-mCherry.
1069 The following genotypes were imaged: wild type (UB35987), Δ*LUTI* (UB35989), *WHI5-*
1070 *AA* (UB35991), Δ*LUTI; WHI5-AA* (UB35989)**.** Quantification as percent of cells that
1071 entered meiosis assayed by nuclear Rec8 appearance. Experiments were performed
1072 using two biological replicates, mean value plotted with range. Differences in meiotic
1073 progression compared by Mann-Whitney test, two-tailed (*, p = 0.0112 [wild type vs.
1074 Δ*LUTI*; *WHI5-AA*]). **F.** Model of SBF regulation during meiotic entry. Ime1 downregulates
1075 Swi4 protein expression via induction of *SWI4^{LUTI}* while Whi5 represses SBF activity in

1076 parallel to LUTI-based mechanism to prevent expression of SBF targets, including G1
1077 cyclins, which perturb meiotic entry via blocking interaction between Ime1 and its cofactor
1078 Ume6.
1079
1080
1081
1082
1083 **REFERENCES**
1084

1085 Abeliovich, H., and D.J. Klionsky. 2001. Autophagy in Yeast: Mechanistic Insights and
1086 Physiological Function. *Microbiol. Mol. Biol. Rev.* 65:463–479.
1087 doi:10.1128/mmbr.65.3.463-479.2001.
1088 Anderson, E.L., A.E. Baltus, H.L. Roepers-Gajadien, T.J. Hassold, D.G. De Rooij,
1089 A.M.M. Van Pelt, and D.C. Page. 2008. Stra8 and its inducer, retinoic acid, regulate
1090 meiotic initiation in both spermatogenesis and oogenesis in mice. *Proc. Natl. Acad.*
1091 *Sci. U. S. A.* 105:14976–14980. doi:10.1073/pnas.0807297105.
1092 Andrews, B.J., and I. Herskowitz. 1989. The yeast SWI4 protein contains a motif
1093 present in developmental regulators and is part of a complex involved in cell-cycle-
1094 dependent transcription. *Nature*. 342:830–833. doi:10.1038/342830a0.
1095 Argüello-Miranda, O., Y. Liu, N.E. Wood, P. Kositangool, and A. Doncic. 2018.
1096 Integration of Multiple Metabolic Signals Determines Cell Fate Prior to
1097 Commitment. *Mol. Cell*. 71:733-744.e11. doi:10.1016/j.molcel.2018.07.041.
1098 Bähler, J., J.Q. Wu, M.S. Longtine, N.G. Shah, A. McKenzie, A.B. Steever, A. Wach, P.
1099 Philippsen, and J.R. Pringle. 1998. Heterologous modules for efficient and versatile
1100 PCR-based gene targeting in Schizosaccharomyces pombe. *Yeast*. 14:943–951.
1101 doi:10.1002/(SICI)1097-0061(199807)14:10<943::AID-YEA292>3.0.CO;2-Y.
1102 Baltus, A.E., D.B. Menke, Y.C. Hu, M.L. Goodheart, A.E. Carpenter, D.G. De Rooij, and
1103 D.C. Page. 2006. In germ cells of mouse embryonic ovaries, the decision to enter
1104 meiosis precedes premeiotic DNA replication. *Nat. Genet.* 38:1430–1434.
1105 doi:10.1038/ng1919.
1106 Bean, J.M., E.D. Siggia, and F.R. Cross. 2005. High functional overlap between MluI
1107 cell-cycle box binding factor and Swi4/6 cell-cycle box binding factor in the G1/S

1108 transcriptional program in Saccharomyces cerevisiae. *Genetics*. 171:49–61.
1109 doi:10.1534/genetics.105.044560.
1110 Berchowitz, L.E., A.S. Gajadhar, F.J. van Werven, A.A. De Rosa, M.L. Samoylova, G.A.
1111 Brar, Y. Xu, C. Xiao, B. Futcher, J.S. Weissman, F.M. White, and A. Amon. 2013. A
1112 developmentally regulated translational control pathway establishes the meiotic
1113 chromosome segregation pattern. *Genes Dev.* 27:2147–2163.
1114 doi:10.1101/gad.224253.113.
1115 Bowdish, K.S., H.E. Yuan, and A.P. Mitchell. 1994. Analysis of RIM11, a yeast protein
1116 kinase that phosphorylates the meiotic activator IME1. *Mol. Cell. Biol.* 14:7909–
1117 7919. doi:10.1128/mcb.14.12.7909-7919.1994.
1118 Bowdish, K.S., H.E. Yuan, and A.P. Mitchell. 1995. Positive control of yeast meiotic
1119 genes by the negative regulator UME6. *Mol. Cell. Biol.* 15:2955–2961.
1120 doi:10.1128/mcb.15.6.2955.
1121 Brar, G.A., M. Yassour, N. Friedman, A. Regev, N.T. Ingolia, and J.S. Weissman. 2012.
1122 High-Resolution View of the Yeast Meiotic Program Revealed by Ribosome
1123 Profiling. *Science (80-.).* 335:552–558. doi:10.1126/science.1215110.
1124 Breitkreutz, A., H. Choi, J.R. Sharom, L. Boucher, V. Neduva, B. Larsen, Z.Y. Lin, B.J.
1125 Breitkreutz, C. Stark, G. Liu, J. Ahn, D. Dewar-Darch, T. Reguly, X. Tang, R.
1126 Almeida, Z.S. Qin, T. Pawson, A.C. Gingras, A.I. Nesvizhskii, and M. Tyers. 2010.
1127 A global protein kinase and phosphatase interaction network in yeast. *Science (80-.*
1128 *).* 328:1043–1046. doi:10.1126/science.1176495.
1129 De Bruin, R.A.M., W.H. McDonald, T.I. Kalashnikova, J. Yates, and C. Wittenberg.
1130 2004. Cln3 activates G1-specific transcription via phosphorylation of the SBF
1131 bound repressor Whi5. *Cell*. 117:887–898. doi:10.1016/j.cell.2004.05.025.
1132 Brush, G.S., N.A. Najor, A.A. Dombkowski, D. Cukovic, and K.E. Sawarynski. 2012.
1133 Yeast ime2 functions early in meiosis upstream of cell cycle-regulated sbf and mbf
1134 targets. *PLoS One*. 7:1–12. doi:10.1371/journal.pone.0031575.
1135 Carlile, T.M., and A. Amon. 2008. Meiosis I Is Established through Division-Specific
1136 Translational Control of a Cyclin. *Cell*. 133:280–291.
1137 doi:10.1016/j.cell.2008.02.032.
1138 Chen, J., D. Mcswiggen, and E. Ünal. 2018. Single Molecule Fluorescence In Situ

1139 Hybridization (smFISH) Analysis in Budding Yeast Vegetative Growth and
1140 Meiosis. 1–14. doi:10.3791/57774.
1141 Chen, J., A. Tresenrider, M. Chia, D.T. McSwiggen, G. Spedale, V. Jorgensen, H. Liao,
1142 F.J. Van Werven, and E. Ünal. 2017. Kinetochore inactivation by expression of a
1143 repressive mRNA. *Elife*. 6:1–31. doi:10.7554/eLife.27417.
1144 Cheng, Z., G.M. Otto, E.N. Powers, A. Keskin, P. Mertins, S.A. Carr, M. Jovanovic, and
1145 G.A. Brar. 2018. Pervasive, Coordinated Protein-Level Changes Driven by
1146 Transcript Isoform Switching during Meiosis. *Cell*. 172:910-923.e16.
1147 doi:10.1016/j.cell.2018.01.035.
1148 Chia, M., A. Tresenrider, J. Chen, G. Spedale, V. Jorgensen, E. Ünal, and F.J. van
1149 Werven. 2017. Transcription of a 5' extended mRNA isoform directs dynamic
1150 chromatin changes and interference of a downstream promoter. *Elife*. 6:1–23.
1151 doi:10.7554/eLife.27420.
1152 Chia, M., and F.J. van Werven. 2016. Temporal Expression of a Master Regulator
1153 Drives Synchronous Sporulation in Budding Yeast. *G3:*
1154 *Genes|Genomes|Genetics*. 6:3553–3560. doi:10.1534/g3.116.034983.
1155 Colomina, N., E. Garí, C. Gallego, E. Herrero, and M. Aldea. 1999. G1cyclins block the
1156 Ime1 pathway to make mitosis and meiosis incompatible in budding yeast. *EMBO*
1157 *J.* 18:320–329. doi:10.1093/emboj/18.2.320.
1158 Costanzo, M., J.L. Nishikawa, X. Tang, J.S. Millman, O. Schub, K. Breitkreuz, D. Dewar,
1159 I. Rupes, B. Andrews, and M. Tyers. 2004. CDK activity antagonizes Whi5, an
1160 inhibitor of G1/S transcription in yeast. *Cell*. 117:899–913.
1161 doi:10.1016/j.cell.2004.05.024.
1162 Van Dalfsen, K.M., S. Hodapp, A. Keskin, G.M. Otto, C.A. Berdan, A. Higdon, T.
1163 Cheunkarndee, D.K. Nomura, M. Jovanovic, and G.A. Brar. 2018. Global Proteome
1164 Remodeling during ER Stress Involves Hac1-Driven Expression of Long
1165 Undecoded Transcript Isoforms. *Dev. Cell*. 46:219-235.e8.
1166 doi:10.1016/j.devcel.2018.06.016.
1167 Dorsey, S., S. Tollis, J. Cheng, L. Black, S. Notley, M. Tyers, and C.A. Royer. 2018.
1168 G1/S Transcription Factor Copy Number Is a Growth-Dependent Determinant of
1169 Cell Cycle Commitment in Yeast. *Cell Syst.* 6:539-554.e11.

1170 doi:10.1016/j.cels.2018.04.012.
1171 Eisenberg, A.R., A.L. Higdon, I. Hollerer, A.P. Fields, I. Jungreis, P.D. Diamond, M.
1172 Kellis, M. Jovanovic, and G.A. Brar. 2020. Translation Initiation Site Profiling
1173 Reveals Widespread Synthesis of Non-AUG-Initiated Protein Isoforms in Yeast.
1174 *Cell Syst.* 11:145-160.e5. doi:10.1016/j.cels.2020.06.011.
1175 Espinoza, F.H., J. Ogas, I. Herskowitz, and D. Morgant. 2016. Cell Cycle Control by a
1176 Complex of the Cyclin HCS26 (PCL1) and the Kinase PHO85 Author (s): F .
1177 Hernan Espinoza , Joseph Ogas , Ira Herskowitz and David O . Morgan Published
1178 by : American Association for the Advancement of Science Stable URL : http://.
1179 266:1388–1391.
1180 Fridy, P.C., Y. Li, S. Keegan, M.K. Thompson, I. Nudelman, J.F. Scheid, M. Oeffinger,
1181 M.C. Nussenzweig, D. Fenyö, B.T. Chait, and M.P. Rout. 2014. A robust pipeline
1182 for rapid production of versatile nanobody repertoires. *Nat. Methods*. 11:1253–
1183 1260. doi:10.1038/nmeth.3170.
1184 Gallego, C., E. Garí, N. Colomina, E. Herrero, and M. Aldea. 1997. The Cln3 cyclin is
1185 down-regulated by translational repression and degradation during the G1 arrest
1186 caused by nitrogen deprivation in budding yeast. *EMBO J.* 16:7196–7206.
1187 doi:10.1093/emboj/16.23.7196.
1188 Gaubatz, S., G.J. Lindeman, S. Ishida, L. Jakoi, J.R. Nevins, D.M. Livingston, and R.E.
1189 Rempel. 2000. E2F4 and E2F5 play an essential role in pocket protein-mediated
1190 G1 control. *Mol. Cell*. 6:729–735. doi:10.1016/S1097-2765(00)00071-X.
1191 Gibson, D.G., L. Young, R.Y. Chuang, J.C. Venter, C.A. Hutchison, and H.O. Smith.
1192 2009. Enzymatic assembly of DNA molecules up to several hundred kilobases. *Nat.*
1193 *Methods*. 6:343–345. doi:10.1038/nmeth.1318.
1194 Harris, A., and E. Ünal. 2023. The transcriptional regulator Ume6 is a major driver of
1195 early gene expression during gametogenesis. *Genetics*. 225:1–21.
1196 doi:10.1093/genetics/iyad123.
1197 Harris, M.R., D. Lee, S. Farmer, N.F. Lowndes, and R.A.M. de Bruin. 2013. Binding
1198 Specificity of the G1/S Transcriptional Regulators in Budding Yeast. *PLoS One*.
1199 8:1–7. doi:10.1371/journal.pone.0061059.
1200 Hartwell, L.H., J. Culotti, J.R. Pringle, and B.J. Reid. 1974. Genetic control of the cell

1201 division cycle in yeast. *Science*. 183:46–51. doi:10.1126/SCIENCE.183.4120.46.
1202 Haruki, H., J. Nishikawa, and U.K. Laemmli. 2008. The Anchor-Away Technique: Rapid,
1203 Conditional Establishment of Yeast Mutant Phenotypes. *Mol. Cell*. 31:925–932.
1204 doi:10.1016/j.molcel.2008.07.020.
1205 Hasan, M., S. Brocca, E. Sacco, M. Spinelli, P. Elena, L. Matteo, A. Lilia, and M.
1206 Vanoni. 2014. A comparative study of Whi5 and retinoblastoma proteins : from
1207 sequence and structure analysis to intracellular networks. 4:1–24.
1208 doi:10.3389/fphys.2013.00315.
1209 Van Den Heuvel, S., and N.J. Dyson. 2008. Conserved functions of the pRB and E2F
1210 families. *Nat. Rev. Mol. Cell Biol.* 9:713–724. doi:10.1038/nrm2469.
1211 Holt, L., B. Tuch, J. Villén, A. Johnson, S. Gygi, and D. Morgan. 2009. Global analysis
1212 of Cdk1 substrate phosphorylation sites provides insights into evolution. *Science*
1213 *(80-.).* 325:1682–1686.
1214 Honigberg, S.M. 2003. Signal pathway integration in the switch from the mitotic cell
1215 cycle to meiosis in yeast. *J. Cell Sci.* 116:2137–2147. doi:10.1242/jcs.00460.
1216 Ishiguro, K. ichiro, K. Matsuura, N. Tani, N. Takeda, S. Usuki, M. Yamane, M.
1217 Sugimoto, S. Fujimura, M. Hosokawa, S. Chuma, M.S.H. Ko, K. Araki, and H. Niwa.
1218 2020. MEIOSIN Directs the Switch from Mitosis to Meiosis in Mammalian Germ
1219 Cells. *Dev. Cell*. 52:429-445.e10. doi:10.1016/j.devcel.2020.01.010.
1220 Iyer, V.R., C.E. Horak, P.O. Brown, D. Botstein, V.R. Iyer, M. Snyder, and C.S. Scafe.
1221 2001. Genomic binding sites of the yeast cell-cycle transcription factors SBF and
1222 MBF. *Nature*. 409:533–538. doi:10.1038/35054095.
1223 Johnston, G.C., J.R. Pringle, and L.H. Hartwell. 1977. Coordination of Growth With Cell
1224 Division. *Exp. Cell Res.* 105:79–98.
1225 Jorgensen, P., and M. Tyers. 2004. How cells coordinate growth and division. *Curr. Biol.*
1226 14:1014–1027. doi:10.1016/j.cub.2004.11.027.
1227 Julian, L.M., Y. Liu, C.A. Pakenham, D. Dugal-Tessier, V. Ruzhynsky, S. Bae, S.Y. Tsai,
1228 G. Leone, R.S. Slack, and A. Blais. 2016. Tissue-specific targeting of cell fate
1229 regulatory genes by E2f factors. *Cell Death Differ.* 23:565–575.
1230 doi:10.1038/cdd.2015.36.
1231 Kadosh, D., and K. Struhl. 1997. Repression by Ume6 involves recruitment of a

1232 complex containing Sin3 corepressor and Rpd3 histone deacetylase to target
1233 promoters. *Cell*. 89:365–371. doi:10.1016/S0092-8674(00)80217-2.
1234 Kassir, Y., D. Granot, and G. Simchen. 1988. IME1, a positive regulator gene of meiosis
1235 in S. cerevisiae. *Cell*. 52:853–862. doi:10.1016/0092-8674(88)90427-8.
1236 Kelliher, C.M., M.W. Foster, F.C. Motta, A. Deckard, E.J. Soderblom, M.A. Moseley, and
1237 S.B. Haase. 2018. Layers of regulation on cell-cycle gene expression in the
1238 budding yeast *Saccharomyces cerevisiae*. *Mol. Biol. Cell*. mbc.E18-04-0255.
1239 doi:10.1091/mbc.E18-04-0255.
1240 Kim, D., J.M. Paggi, C. Park, C. Bennett, and S.L. Salzberg. 2019. Graph-based
1241 genome alignment and genotyping with HISAT2 and HISAT-genotype. *Nat.*
1242 *Biotechnol.* 37:907–915. doi:10.1038/s41587-019-0201-4.
1243 Klein, F., P. Mahr, M. Galova, S.B.C. Buonomo, C. Michaelis, K. Nairz, and K. Nasmyth.
1244 1999. A Central Role for Cohesins in Sister Chromatid Cohesion, Formation of
1245 Axial Elements, and Recombination during Yeast Meiosis Genetic and biochemical
1246 analyses have identified. *Cell*. 98:91–103.
1247 Kojima, M.L., D.G. De Rooij, and D.C. Page. 2019. Amplification of a broad
1248 transcriptional program by a common factor triggers the meiotic cell cycle in mice.
1249 *Elife*. 8:1–32. doi:10.7554/eLife.43738.
1250 Love, M.I., W. Huber, and S. Anders. 2014. Moderated estimation of fold change and
1251 dispersion for RNA-seq data with DESeq2. *Genome Biol.* 15:1–21.
1252 doi:10.1186/s13059-014-0550-8.
1253 Malathi, K., Y. Xiao, and A.P. Mitchell. 1997. Interaction of yeast repressor-activator
1254 protein Ume6p with glycogen synthase kinase 3 homolog Rim11p. *Mol. Cell. Biol.*
1255 17:7230–7236. doi:10.1128/mcb.17.12.7230.
1256 Malathi, K., Y. Xiao, and A.P. Mitchell. 1999. Catalytic roles of yeast GSK3β/shaggy
1257 homolog Rim11p in meiotic activation. *Genetics*. 153:1145–1152.
1258 doi:10.1093/genetics/153.3.1145.
1259 Mcinerny, C.J., J.F. Partridge, G.E. Mikesell, D.P. Creemer, and L.L. Breeden. 1997. A
1260 novel Mcml-dependent element in the WI4 , CLN3 , CDC6 , and CDC4S7
1261 promoters activates M / Gi-specific transcription. *Genes Dev.* 1277–1288.
1262 doi:10.1101/gad.11.10.1277.

1263 Miller, M.P., E. Ünal, G.A. Brar, and A. Amon. 2012. Meiosis I chromosome segregation
1264 is established through regulation of microtubule-kinetochore interactions. *Elife*.
1265 2012:1–30. doi:10.7554/eLife.00117.
1266 Moreno-Torres, M., M. Jaquenoud, M.P. Péli-Gulli, R. Nicastro, and C. De Virgilio. 2017.
1267 TORC1 coordinates the conversion of Sic1 from a target to an inhibitor of cyclin-
1268 CDK-Cks1. *Cell Discov.* 3:1–12. doi:10.1038/celldisc.2017.12.
1269 Parviz, F., and W. Heideman. 1998. Growth-independent regulation of CLN3 mRNA
1270 levels by nutrients in Saccharomyces cerevisiae. *J. Bacteriol.* 180:225–230.
1271 doi:10.1128/jb.180.2.225-230.1998.
1272 Pertea, M., G.M. Pertea, C.M. Antonescu, T.C. Chang, J.T. Mendell, and S.L. Salzberg.
1273 2015. StringTie enables improved reconstruction of a transcriptome from RNA-seq
1274 reads. *Nat. Biotechnol.* 33:290–295. doi:10.1038/nbt.3122.
1275 Pnueli, L., I. Edry, M. Cohen, and Y. Kassir. 2004. Glucose and Nitrogen Regulate the
1276 Switch from Histone Deacetylation to Acetylation for Expression of Early Meiosis-
1277 Specific Genes in Budding Yeast. *Mol. Cell. Biol.* 24:5197–5208.
1278 doi:10.1128/mcb.24.12.5197-5208.2004.
1279 Primig, M., R.M. Williams, E.A. Winzeler, G.G. Tevzadze, A.R. Conway, S.Y. Hwang,
1280 R.W. Davis, and R.E. Esposito. 2000. The core meiotic transcriptome in budding
1281 yeasts. *Nat. Genet.* 26:415–423. doi:10.1038/82539.
1282 Raj, A., P. van den Bogaard, S.A. Rifkin, A. van Oudenaarden, and S. Tyagi. 2008.
1283 Imaging individual mRNA molecules using multiple singly labeled probes. *Nat.*
1284 *Methods*. 5:877–879. doi:10.1038/nmeth.1253.
1285 Rubin-Bejerano, I., S. Mandel, K. Robzyk, and Y. Kassir. 1996. Induction of meiosis in
1286 Saccharomyces cerevisiae depends on conversion of the transcriptional represssor
1287 Ume6 to a positive regulator by its regulated association with the transcriptional
1288 activator Ime1. *Mol. Cell. Biol.* 16:2518–2526. doi:10.1128/mcb.16.5.2518.
1289 Rundlett E., S., A. Carmen A., N. Suka, B. Turner M., and M. Grunstein. 2003.
1290 Transcriptional repression byUME6 involves deacetylationof lysine5 of
1291 histoneH4byRPD3. *Nature*. 426:181–186.
1292 Schindelin, J., I. Arganda-Carreras, E. Frise, V. Kaynig, M. Longair, T. Pietzsch, S.
1293 Preibisch, C. Rueden, S. Saalfeld, B. Schmid, J.Y. Tinevez, D.J. White, V.

1294 Hartenstein, K. Eliceiri, P. Tomancak, and A. Cardona. 2012. Fiji: An open-source
1295 platform for biological-image analysis. *Nat. Methods*. 9:676–682.
1296 doi:10.1038/nmeth.2019.
1297 Sidorova, J.M., and L.L. Breeden. 2002. Precocious S-phase entry in budding yeast
1298 prolongs replicative state and increases dependence upon Rad53 for viability.
1299 *Genetics*. 160:123–136.
1300 Simon, I., J. Barnett, N. Hannett, C.T. Harbison, N.J. Rinaldi, T.L. Volkert, J.J. Wyrick, J.
1301 Zeitlinger, D.K. Gifford, T.S. Jaakkola, and R.A. Young. 2001. Serial Regulation of
1302 Transcriptional Regulators in the Yeast Cell Cycle. 106:697–708.
1303 Smith, H.E., S.E. Driscoll, R.A.L. Sia, H.E. Yuan, and A.P. Mitchell. 1993. Genetic
1304 evidence for transcriptional activation by the yeast IME1 gene product. *Genetics*.
1305 133:775–784. doi:10.1093/genetics/133.4.775.
1306 Smolka, M.B., F.M. Bastos De Oliveira, M.R. Harris, and R.A.M. De Bruin. 2012. The
1307 checkpoint transcriptional response: Make sure to turn it off once you are satisfied.
1308 *Cell Cycle*. 11:3166–3174. doi:10.4161/cc.21197.
1309 Spellman, P., G. Sherlock, M. Zhang, V. Iyer, K. Anders, M. Eisen, P. Brown, D.
1310 Botstein, and B. Futcher. 1998. Comprehensive identification of cell cycle-regulated
1311 genes of the yeast Saccharomyces cerevisiae by microarray hybridization. *Mol.*
1312 *Biol. Cell*. 9:3273–3297. doi:10.1091/mbc.9.12.3273.
1313 Subramanian, A., P. Tamayo, V.K. Mootha, S. Mukherjee, B.L. Ebert, M.A. Gillette, A.
1314 Paulovich, S.L. Pomeroy, T.R. Golub, E.S. Lander, and J.P. Mesirov. 2005. Gene
1315 set enrichment analysis: A knowledge-based approach for interpreting genome-
1316 wide expression profiles. *Proc. Natl. Acad. Sci. U. S. A.* 102:15545–15550.
1317 doi:10.1073/pnas.0506580102.
1318 Talarek, N., E. Cameroni, M. Jaquenoud, X. Luo, S. Bontron, S. Lippman, G. Devgan,
1319 M. Snyder, J.R. Broach, and C. De Virgilio. 2010. Initiation of the TORC1-
1320 Regulated G0 Program Requires Igo1/2, which License Specific mRNAs to Evade
1321 Degradation via the 5′-3′ mRNA Decay Pathway. *Mol. Cell*. 38:345–355.
1322 doi:10.1016/j.molcel.2010.02.039.
1323 Tresenrider, A., K. Morse, V. Jorgensen, M. Chia, H. Liao, F.J. van Werven, and E.
1324 Ünal. 2021. Integrated genomic analysis reveals key features of long undecoded

1325 transcript isoform-based gene repression. *Mol. Cell*. 81:2231-2245.e11.
1326 doi:10.1016/j.molcel.2021.03.013.
1327 Tresenrider, A., and E. Ünal. 2017. One-two punch mechanism of gene repression: a
1328 fresh perspective on gene regulation. *Curr. Genet.* 0:1–8. doi:10.1007/s00294-017-
1329 0793-5.
1330 Vidan, S., and A.P. Mitchell. 1997. Stimulation of yeast meiotic gene expression by the
1331 glucose-repressible protein kinase Rim15p. *Mol. Cell. Biol.* 17:2688–2697.
1332 doi:10.1128/mcb.17.5.2688.
1333 Wagner, M. V., M.B. Smolka, R.A.M. de Bruin, H. Zhou, C. Wittenberg, and S.F. Dowdy.
1334 2009. Whi5 regulation by site specific CDK-phosphorylation in Saccharomyces
1335 cerevisiae. *PLoS One*. 4. doi:10.1371/journal.pone.0004300.
1336 Vander Wende, H.M., M. Gopi, M. Onyundo, C. Medrano, T. Adanlawo, and G.A. Brar.
1337 2022. Meiotic resetting of the cellular Sod1 pool is driven by protein aggregation,
1338 degradation, and transient LUTI-mediated repression. *J. Cell Biol.* 222.
1339 doi:10.1101/2022.06.28.498006.
1340 van Werven, F.J., and A. Amon. 2011. Regulation of entry into gametogenesis. *Philos.*
1341 *Trans. R. Soc. B Biol. Sci.* 366:3521–3531. doi:10.1098/rstb.2011.0081.
1342
1343
1344

Supplemental Figure Legends

S1. Swi4 and Ime1 protein abundance, Related to Figure 1

A. Wild type (UB22199) and *pATG8-SWI4* (UB22226) cells collected between 0-4 h in SPO. Immunoblot performed using α-V5 to quantify Swi4-3V5 abundance. Normalized to Hxk2 loading control. **B.** Quantification of the immunoblot in (A). **C.** Immunoblot using α-GFP to quantify GFP-Ime1 abundance. Normalized to Hxk2 loading control. **D.** Quantification of the immunoblot in (C).

S2. Gene ontology analysis for mRNA-seq comparing *pATG8-SWI4* to wild type, Related to Figure 2

A. Gene ontology analysis for genes that have significant increased expression by DESeq2 (see Materials and Methods) in *pATG8-SWI4* (UB2226) and wild type (UB22199*)*. Term size is the number of genes within a defined term. Enrichment score calculated for each term and plotted. **B.** same as in (A) but for genes that have significant decreased expression.

S3. Meiotic entry upon removal of either Cln1 or Cln2, Related to Figure 3

A. Live-cell imaging of meiotic cells marked by Rec8-GFP and nuclear marker Htb1-mCherry, with the following genotypes: wild type (UB32085), *pATG8-SWI4* (UB32089)*, cln2*Δ (UB35595), and *cln1*Δ (UB35597). Quantification of cells that entered meiosis assayed by the initial timing of nuclear Rec8 appearance. Experiments were performed using two biological replicates, mean value plotted with range. A total number of 800 cells were analyzed.

S4. Ime1 protein levels when C*LN2* is overexpressed and rescue of I*ME1* transcript levels and protein abundance with *pCUP1-IME1*, Related to Figure 4

A. Immunoblot was performed on wild type (UB22199) and *pATG8-CLN2* (UB35106) cells collected between 0-6 h in SPO. Immunoblotted using α-GFP to quantify GFP-Ime1 abundance. Normalized to Hxk2 loading control. Representative blots from one of two biological replicates are shown. All blots in this figure were performed the same way. **B.** Quantification of the immunoblot in (A). **C.** RT-qPCR was performed on *IME1* transcript

for samples collected in (A). Quantification was performed in reference to levels of meiotic housekeeping gene *PFY1* and then normalized to wild type. FC = fold change. Experiments were performed in duplicate, mean value plotted with range. **D.** Same as in (C) but for *pCUP1-GFP-IME1* (UB34641) and *pCUP1-GFP-IME1*; *pATG8-CLN2* (UB35057). **E.** Immunoblot was performed on samples from wild type (UB22199)*, pATG8-CLN2* (UB35106), *pCUP1-GFP-IME1* (UB34641), and *pCUP1-GFP-IME1*; *pATG8-CLN2* (UB35057) strains collected between 0-4 h in SPO. 50 μM $CuSO_4$ after 2 h in SPO was added to all cells. Representative blots from one of two biological replicates are shown. **F.** Quantification of the immunoblot in (E).

S5. Expression of *SWI4^{LUTI}* in Ume6(T99N) mutant, Related to Figure 5

Fold change expression in wild type or Ume6(T99N) mutant between pre meiotic conditions and meiotic prophase (Tresenrider et al., 2021).

S6. Whi5 localization in early meiosis, Swi4 protein levels matching Figure 6A, 6C, 6D, and GSEA data for Δ*LUTI*; WHI5-AA, Related to Figure 6

A. Fixed imaging of cells marked with GFP-Ime1 and Whi5-mCherry with DNA stained with DAPI. Representative images with merge at 0 h and 2 h in SPO. Representative cells outlined. **B.** Left: Cells with the following genotypes were collected between 0-6 h in SPO: wild type (UB27083), Δ*LUTI* (UB26874), *WHI5-AA* (UB25431), Δ*LUTI; WHI5-AA* (UB25428). Immunoblotted using α-V5 to quantify Swi4-3V5 abundance. Normalized to Hxk2 loading control. Representative blots from one of two biological replicates are shown. Right: Quantification of blots. **C.** GSEA analysis of mRNA-seq comparing wildtype vs. Δ*LUTI; WHI5-AA (UB25428)* cells collected at 2 h in SPO. Vertical black bars represent early meiotic gene cluster from (Brar et al., 2012) or SBF cluster from (Iyer et al., 2001). The heatmap indicates genes that are more enriched in Δ*LUTI; WHI5-AA* (red, left-side) or genes that are enriched with wild type (blue, right-side). NES = normalized enrichment score. Enrichment was determined comparing wild type to Δ*LUTI; WHI5-AA.*

Supplement Table 1.

Table of differentially expressed genes (DESeq2) plotted in Figure 2F for *pATG8-SWI4* (UB22226) vs. wild type (UB22199).

Supplement Table 2.

Sporulation efficiency of cells at 24 h in SPO media for Rec8-GFP (UB32085*)*, Rec8-GFP; *pATG8-SWI4* (UB32089). 200 cells counted per strain. Second table is sporulation efficiency of cells at 24 h in SPO media for the following genotypes: wild type (UB22199), *pATG8-CLN1* (UB32820), *pATG8-CLN2* (UB25959), *pCUP-GFP-IME1* (UB34641), *pCUP1-GFP-IME1; pATG8-CLN2* (UB35057), *PUS1-αGFP* (UB35593), *PUS1-αGFP; pATG8-CLN2* (UB35982), *UME6-αGFP* (UB35300), and *UME6-αGFP; pATG8-CLN2* (UB35177).

Supplement Table 3.

Table of differentially expressed genes (DESeq2) plotted in Figure 6A, 6C, and 6D. First tab is *WHI5-AA*; Δ*LUTI* vs. wild type. Second tab is *WHI5-AA* vs. wild type. Third tab is Δ*LUTI* versus wild type.

Supplement Table 4.

The genotypes of the strains used in this study.

Supplement Table 5.

Plasmids used in this study.

Supplement Table 6.

Primers used for qPCR and RNA blotting in this study.

Supplemental Table 7.

Image acquisition information.

Su et al_Figure 1

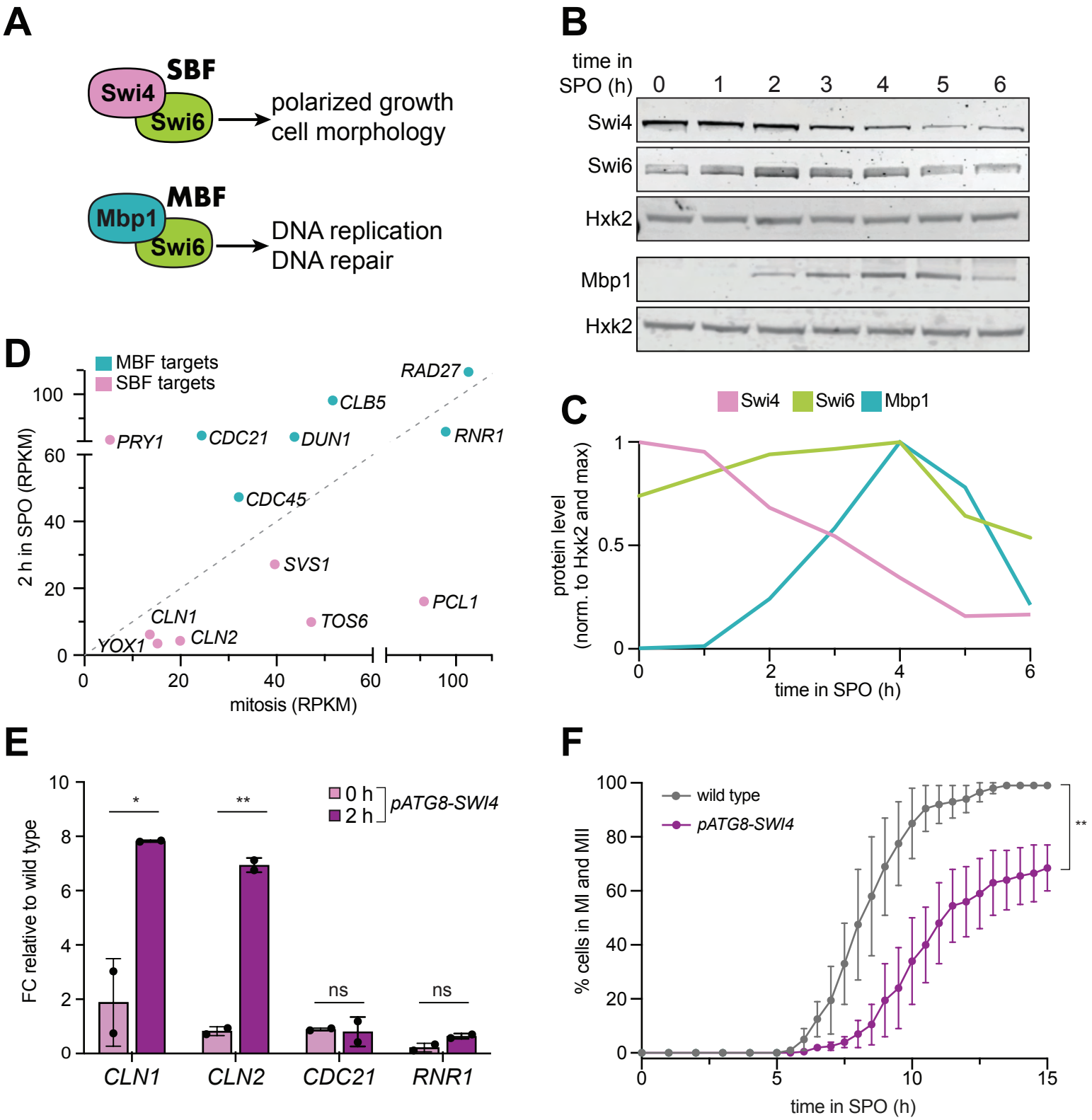

Su et al_Figure 2

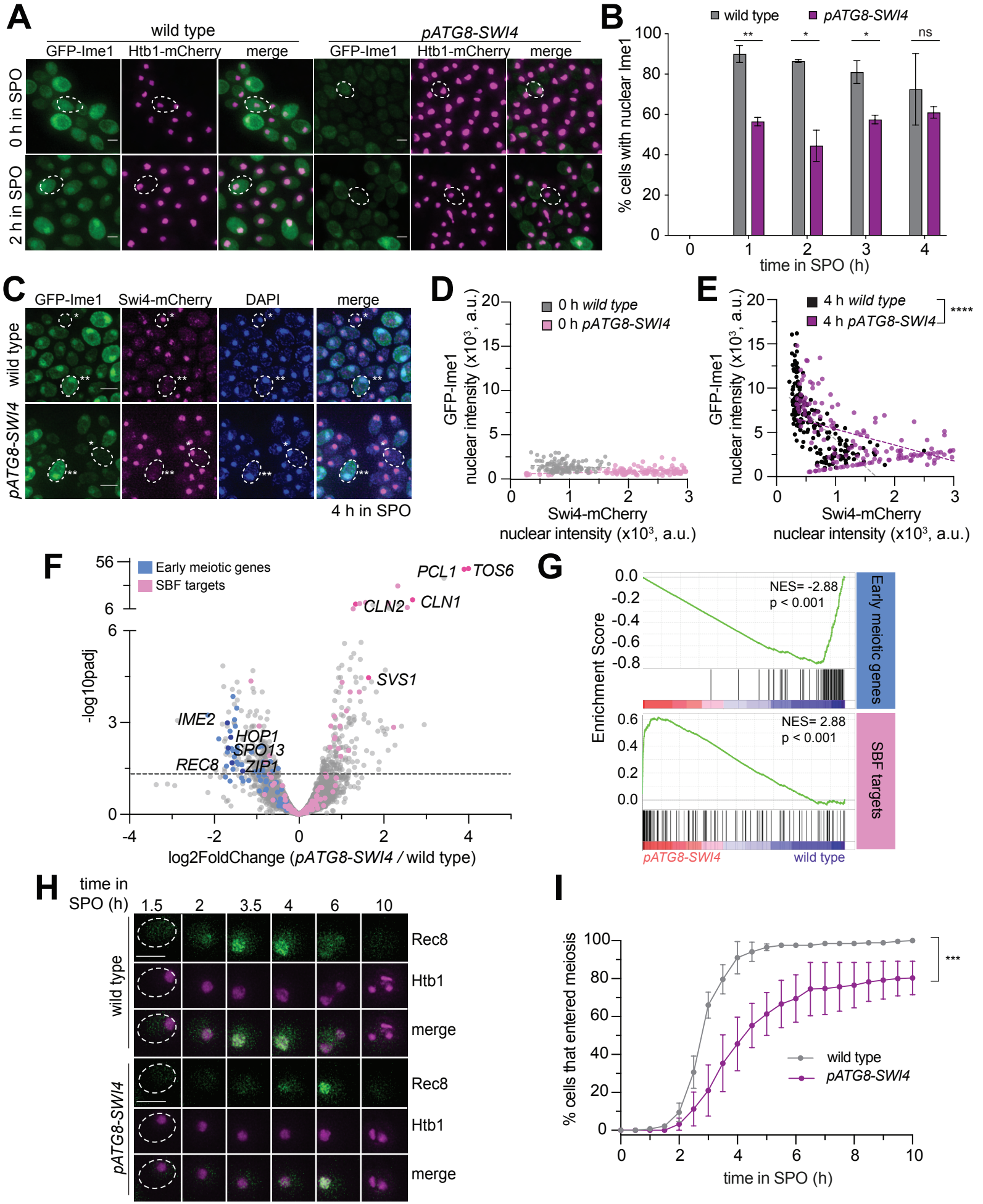

Su et al_Figure 3

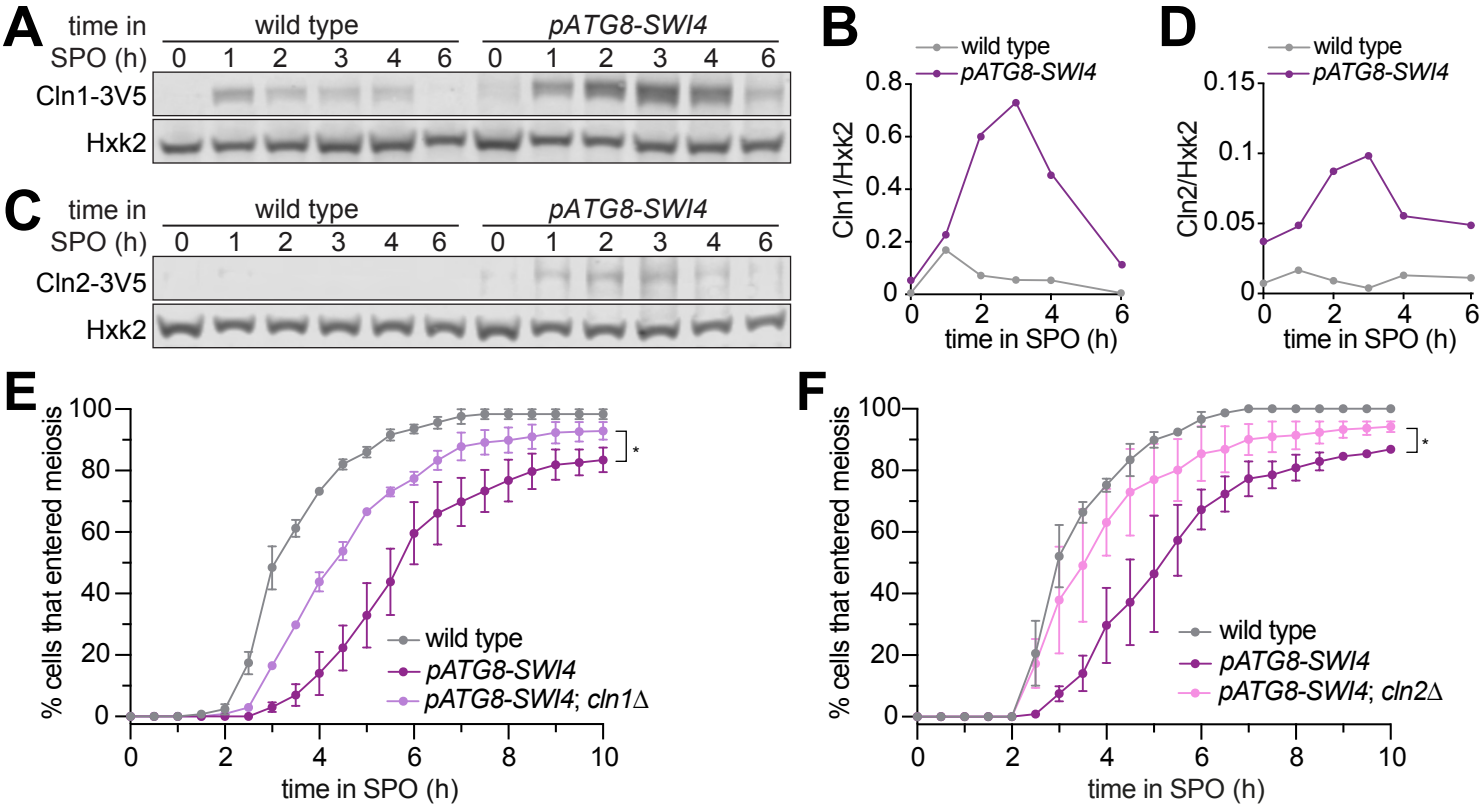

Su et al_Figure 4

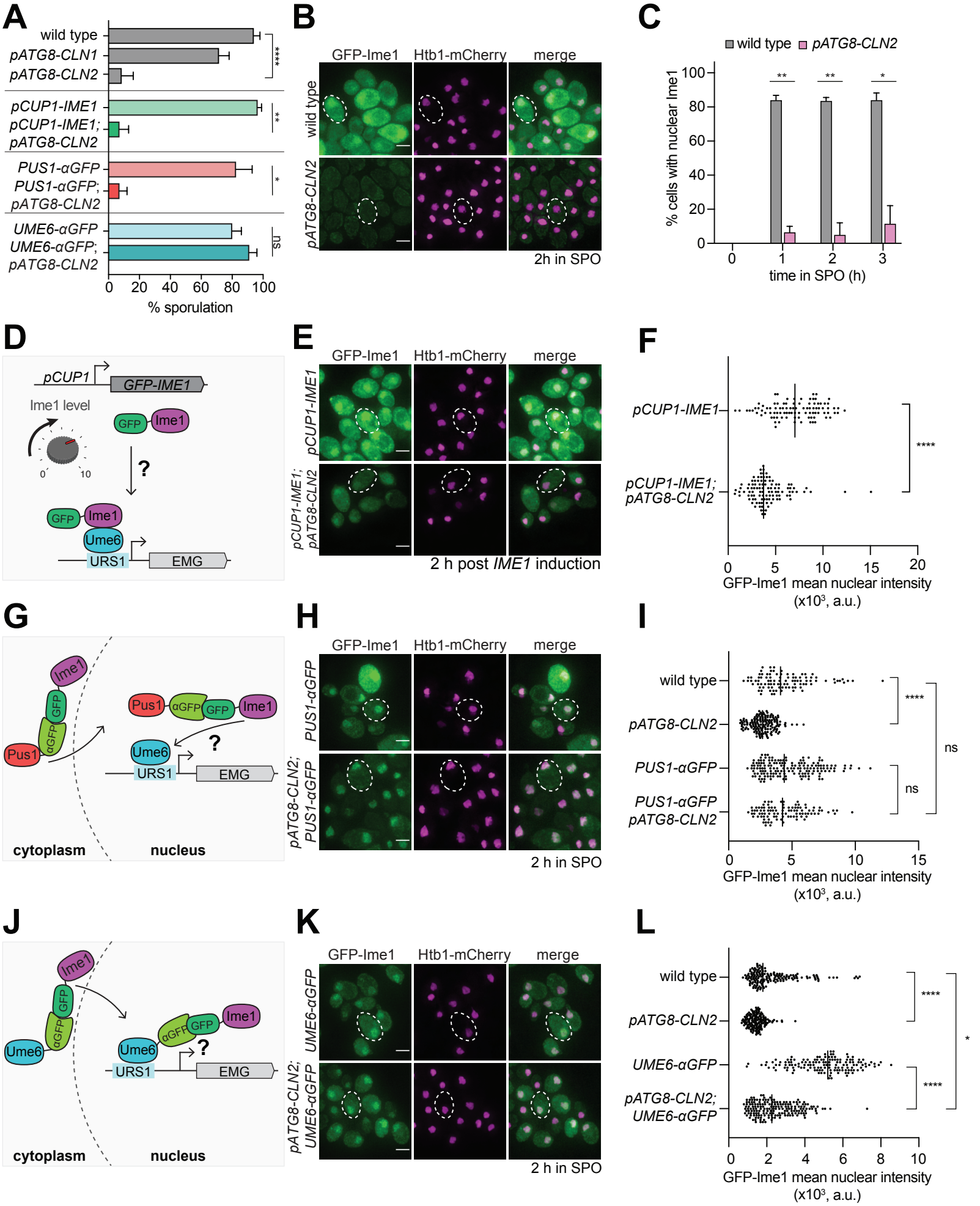

Su et al_Figure 5

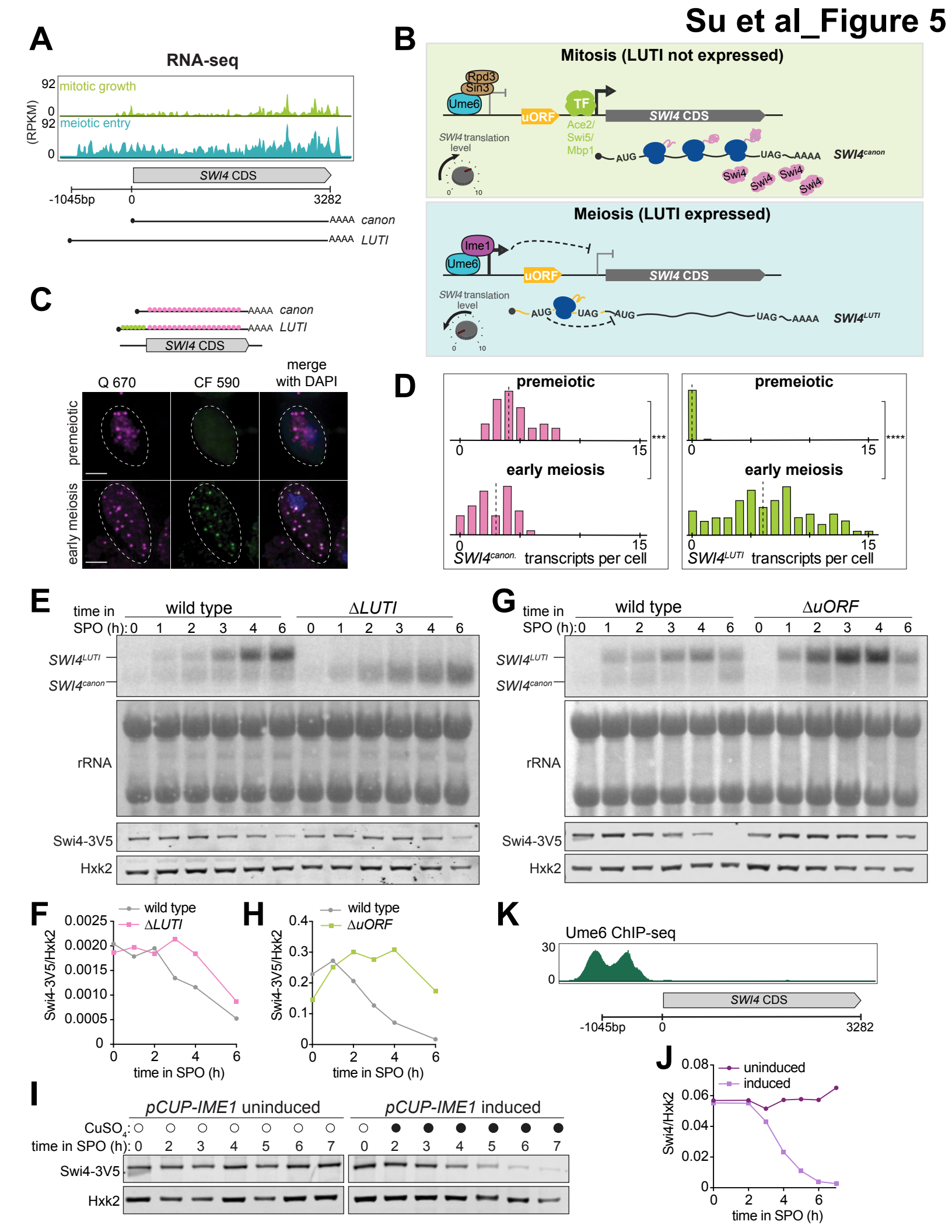
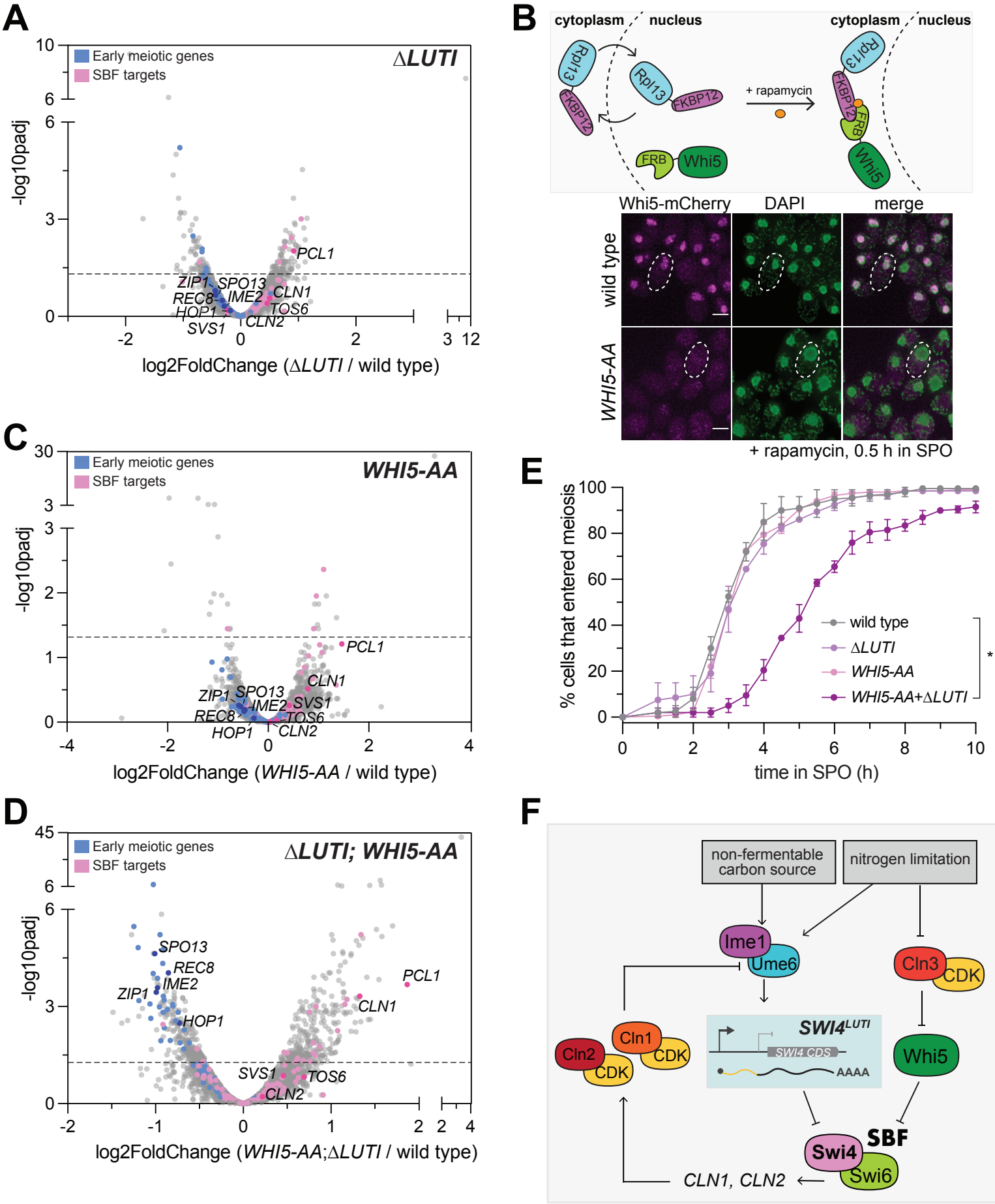
Su et al_Figure 6